Studying the effect of Dark Matter and Galaxy Shape on Supermassive Black Hole Mass measurements using triaxial Schwarzschild Modelling

A Thesis

submitted to
Indian Institute of Science Education and Research Pune
in partial fulfillment of the requirements for the
BS-MS Dual Degree Programme

by

Anirban Roy Chowdhury
Roll No. 20191141

Indian Institute of Science Education and Research Pune
Dr. Homi Bhabha Road,
Pashan, Pune 411008, INDIA.

March, 2024

Supervisor(s): Dr. Sabine Thater, Prof. Prasad Subramanian

Certificate

This is to certify that this dissertation entitled Studying the effect of Dark Matter and Galaxy Shape on Supermassive Black Hole Mass measurements using triaxial Schwarzschild Modelling towards the partial fulfilment of the BS-MS dual degree programme at the Department of Astrophysics, University of Vienna as well as the Indian Institute of Science Education and Research, Pune represents study/work carried out by Anirban Roy Chowdhury at Indian Institute of Science Education and Research under the supervision of Dr. Sabine Thater , Department of Astrophysics, University of Vienna, Austria and Prof. Prasad Subramanian , Department of Physics IISER Pune, during the academic year 2023-2024.

Dr. Sabine Thater Prof. Prasad Subramanian

Committee:
Dr. Sabine Thater
Prof. Prasad Subramanian
Prof. Arka Banerjee

This thesis is dedicated to Appoopan, who inspired my love for astronomy.

Declaration

I hereby declare that the matter embodied in the report entitled ”Studying the effect of Dark Matter and Galaxy Shape on Supermassive Black Hole Mass measurements using triaxial Schwarzschild Modelling ” are the results of the work carried out by me at the Department of Physics, Indian Institute of Science Education and Research, Pune, under the supervision of Dr. Sabine Thater and Prof. Prasad Subramanian and the same has not been submitted elsewhere for any other degree.

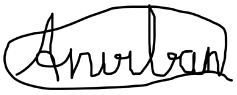

Anirban Roy Chowdhury

Acknowledgments

First and foremost, I would like to thank my parents for their continued support throughout my life leading up to the thesis as well as during this period. Their encouraging words and valuable advice enabled me to overcome many difficulties. It would not have been possible for me to get this far without their help. I would also like to thank my supervisors, Dr. Sabine Thater and Prof. Prasad Subramanian, without whom the thesis would have been impossible. Their guidance and expertise in the field gave me crucial support and direction for my work. Dr. Sabine would offer advice and guidance in weekly meetings that helped me stay on course to complete my thesis as well as provide an avenue to regularly address my doubts and questions, enhancing my overall knowledge. I would also like to thank the entire Dynamics of Stellar Systems Group in Vienna, for providing a friendly and welcoming environment and letting me feel comfortable and welcome when I was otherwise alone in a foreign country. In particular, I would like to thank Shelley, who was a wonderful office mate and helped me get around and understand the University's workings in my first days, and provided excellent company. I would also like to thank Mali and Dr. Ryan Leaman, who were present in many of our weekly meetings with Dr. Sabine and helped me in my project as well as write my thesis. Dr. Ryan gave insightful feedback on my thesis as well as helped me read and understand a lot of relevant background literature. Mali, who was working on her thesis concurrently with mine, and her own research and thesis writing gave me a lot of inspiration to do my own. Finally, I would like to thank my friends in IISER, whose support and camaraderie meant the world to me in this year. Even though many of us were large distances and continents apart, our friendship remained strong. Soumyodeep, Reetish, Parijat, Jason, Akash, Arya, Namasi, Likhith, Sanjana, Ritvee, Krishna and of course, Ace, are just some of the names that made this tumultuous year a joy to get through.

Abstract

In this thesis, the masses of the Supermassive Black Holes of three early-type galaxies are measured using triaxial Schwarzschild Modelling. Particularly, this model includes a triaxial shape parametrization and dark matter, two significant parts of a general early-type galaxy that a previous study [1] lacked but also studied the same sample. This study aims to find how the inclusion of triaxiality and dark matter affects the black hole mass measurement, as well as perform a consistency check for DYNAMITE, a dynamical modelling software developed at the University of Vienna. Three galaxies from the SMASHING sample are used, which have large-scale as well as high resolution IFU data of the center. Schwarzschild modelling confirms that these galaxies are very close to axisymmetric, and their measured SMBH masses are consistent with scaling relations as well as [1]. Inconsistencies with [1] are found in the best-fit values for Mass-to-Light Ratio which requires further study. Dark matter remains poorly constrained by dynamical modelling due to our use of stellar kinematics, but show low best-fit values in this study.

Contents

List of Figures

List of Tables

Chapter 1

Introduction

1.1 Galaxies

Galaxies are vast and ancient structures found throughout the universe. Found in matter overdensities of the universe, each galaxy is home to billions of stars and has an intricate and complex structure. Every galaxy can be one of a vast variety of morphological types and can show a host of different properties. In order to understand the complex interplay between the central Supermassive Black Hole (SMBH) and the host galaxy, it is essential that we also understand other properties of the galaxy, which are all interconnected.

1.1.1 Morphological Type

With the vast variety of galaxies seen by astronomers, it is useful to classify them into types for ease of study. The most common classification for galaxies is the Hubble sequence. Designed by Edwin Hubble [2], it was thought to be an evolutionary sequence, where diffusion-dominated galaxies (called elliptical galaxies) would eventually take one of two evolutionary pathways and transform into either spiral galaxies with bars or without bars. This can be depicted in the form of the famous Tuning Fork diagram shown in Figure 1.1. Now, we know that galaxy evolution is a much more complex topic, and is still an area of active research.

While current astronomers no longer believe that the Hubble sequence is an evolutionary sequence, the conventions created by Hubble still persist to this day. Elliptical galaxies (From E0 to E7 in the Hubble sequence) along with lenticulars (S0) are sometimes referred to as early-type galaxies while spirals are referred to as late-type galaxies. Classification also becomes much more difficult when we take into account the image of the galaxy we see in different wavelength ranges. Structures and shapes we see in a particular wavelength range may not be visible at all in other wavelength ranges. Due to the wealth of different substructures found in galaxies, classification can also depend on what structure is deemed important. For example, the Hubble sequence places great importance on the existence/non-existence of prominent bars. The De Vaucouleur's classification [3] extends the Hubble Sequence and adds three new types: Sd, Sm and

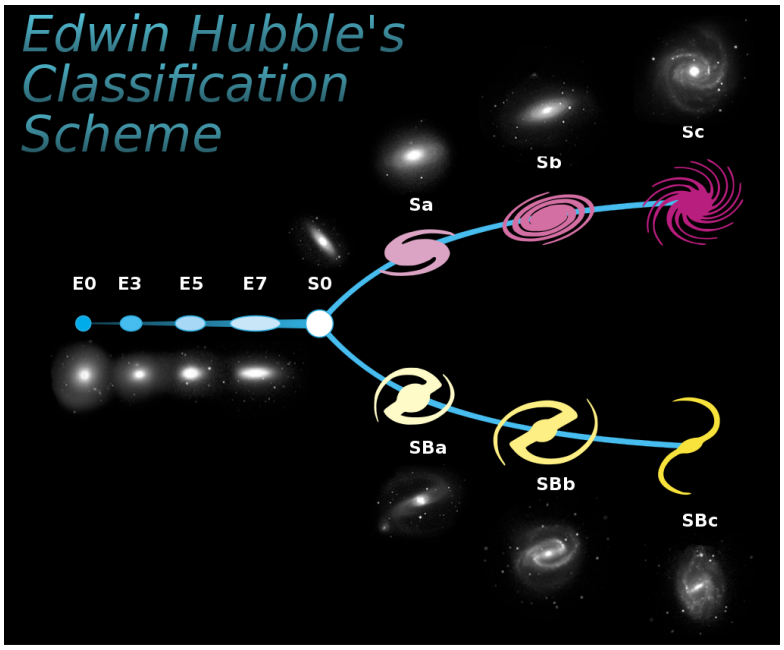

Figure 1.1: This Diagram shows the Hubble sequence. E represents elliptical galaxies, the top fork represents unbarred spirals while the bottom fork represents barred spirals. The meeting point of the three branches is S0, called lenticular galaxies, which are galaxies with a visible disk but no spiral arms(Source: Wikipedia: Hubble Sequence)

Im, keeping the Elliptical classification mostly unchanged. This classification scheme puts more emphasis on ring structures for classification, such as nuclear rings and outer rings. Later classification schemes also followed a similar vein, adding minor changes and shifts in the 'important' substructures.

As useful as morphological classification is, it has some important flaws that must be kept in mind. Any morphological classification scheme is inherently dependent on the spatial orientation of the galaxy relative to us. For example, it is difficult to determine the presence and prominence of a bar in a spiral if the galaxy is edge-on (The axis of rotation is perpendicular to the line of sight). Morphological classification also completely disregards spectroscopic information and is only done using photometric information. As our technology improves, we are also able to see galaxies at larger and larger distances and get more deep imaging to see the outskirts of galaxies, but having high spatial resolution for very distant galaxies still remains extremely difficult [4] or impossible. With almost no knowledge of the detailed structure of these galaxies, it is not possible to assign most of them to distinct morphological types. Furthermore, in focusing on one or more important structural components for classification, the remaining structures and the mechanisms by which they are formed and stabilized are lost, and often two galaxies with very different evolutionary histories may be grouped in the same morphological type. An example of an alternate form of classification is based on color. The color of a galaxy comes from the stellar populations present in it, while the morphological type depends mostly on the dynamics of the constituent stars or gas. For example, a redder galaxy indicates that it is composed of older stars, with a low star for-

mation rate. A bluer galaxy, on the other hand, is indicative of a population consisting of younger stars, and additional spectroscopic information confirming the presence of large amounts of cold gas will indicate a higher star formation rate [5]. Thus, color classification provides much better insight into the galaxy's evolutionary history, and since it doesn't depend on highly resolved images of the galaxy, can be applied reasonably well to galaxies at very high distances. (After correcting for the cosmological redshift!)

Color classification is still not without flaws. For one, there isn't a perfect overlap between galaxy structure and color. There can be very red spiral galaxies and very blue elliptical galaxies. Another important point is that there are a number of different evolutionary pathways that galaxies may take to reach their current state, and may have very similar colors, but are bound to have very different structures.

Despite the flaws, we have found some interesting correlations between morphological types of galaxies and their stellar populations. Elliptical galaxies tend to have very low amounts of cold gas and old stellar populations, made of redder stars. On the other hand, spiral galaxies tend to have high amounts of gas, and the ones with large amounts of cold gas have younger populations with bluer stars. This gives us insight into their evolutionary history as well. The most common method of formation of ellipticals is thought to be via the collision of spiral galaxies [6]. Such a violent event strips the light gas away from the galactic centre, and after an initial increase in star formation caused by the initial merger, there is a lack of cold gas available for continued star formation, and it quickly stops. Galaxy formation through mergers (or collisions) has two major phases: in-situ and accretion. More details are discussed in [6].

1.1.2 Galaxy structure

As discussed in the previous section, galaxies have a number of different structural components, depending on the dynamics of the stars and gas (or occasionally even the central AGN). While there is no shortage of distinct structures in spiral galaxies (which usually have much more prominent substructures) like bars, disks, bulges, spiral arms, rings etc., since this work deals exclusively with elliptical and lenticular galaxies, we shall restrict discussion to only these types of galaxies from this point on.

Compared to spiral galaxies, elliptical galaxies mostly possess very little to no substructure (that our current telescopes can easily detect. Substructures in very close ellipticals can still be seen). Ellipticals have a much larger bulge as a result of being diffusion dominated. That is why a single relation is enough to reasonably quantify the brightness profile of many elliptical galaxies. The De Vaucouleur's Profile [7] (which is a profile of the proejcted light distribution) describes the radial profile of apparent magnitude falling off as $R^{1/4}$. This simple law is accurate for a large number of ellipticals (except at very large radii and at the very center). The deviations from the De Vaucouleur's Profile in the galactic center provide another form of classification for ellipticals. Galaxies with a lower brightness than the expected value from the De Vaucouleur's Profile at the center are especially luminous galaxies. These galaxies are said

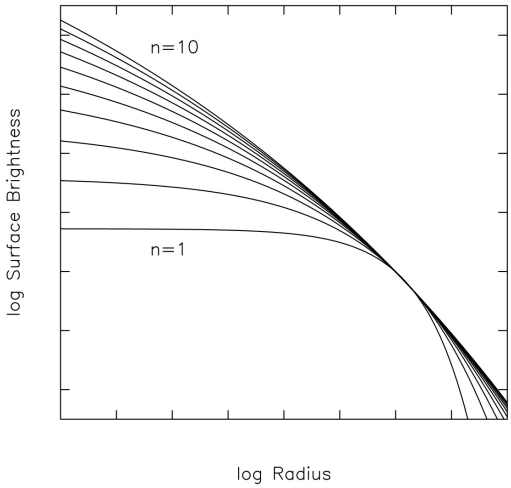

Figure 1.2: This figure shows Sersic Profiles for different indices (n). n=4 shows a De Vaucouleur's Profile

to have a distinct core. Conversely, galaxies with a higher brightness than expected at the center are usually quite dim compared to most ellipticals.

For other ellipticals, however, a De Vaucouleur's Profile is insufficient to describe the surface brightness profile. A more general form of a surface brightness profile is a Sersic Profile[8], where the apparent magnitude is described to follow a $R^{1/n}$ trend, where n is called the Sersic index. Astronomers today even model brightness profiles with multiple Sersic profiles, with different Sersic Indices depending on the radius. This becomes important, especially for more lenticular galaxies whose disks would not follow the same brightness profile as the inner bulge.

Another important part of the structure of an elliptical is its shape. An elliptical galaxy can be modelled very well as a collisionless gas with stars as its particles. So the question becomes: if this galaxy sits in empty space, why is it not spherical? The net rotation of the galaxy plays a big part in the deviation from a sphere. The centrifugal force forces it to become wider perpendicular to the axis of rotation. But elliptical galaxies are *triaxial* in general [9] (See Figure 1.3). That means that the axis length of the ellipsoid is different along all three directions. An axisymmetric case is when two axes are equal in length, and when all three axes are the same, it becomes a sphere. Although one would expect ellipticals to always be axisymmetric (or flattened spheres, like the earth) due to their rotation, we find that their rotational velocities are not high enough to explain their shape. In fact, even purely axisymmetric galaxies do not have shapes that are purely supported by rotation. The shape of the galaxy is hence not a consequence of its rotational dynamics, but rather due to the expected equilibrium distribution of the stellar orbits and their velocities. These orbits can be highly complex and are not necessarily closed [10]. See [11] for more details on shape of early-type galaxies.

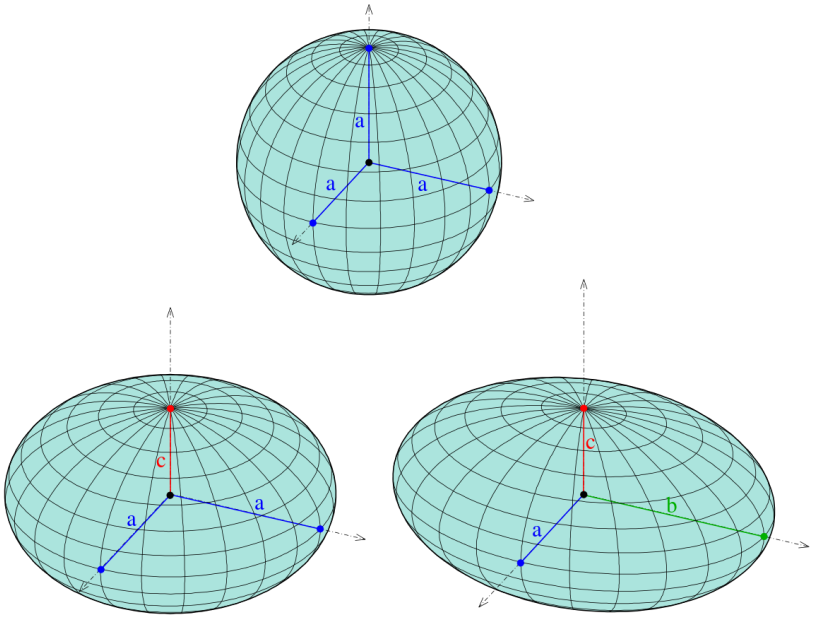

Figure 1.3: This figure shows the three different kinds of ellipsoid shapes that elliptical galaxies might have. The first shape (top row) is a sphere, with a constant radius a. The second shape (bottom row, left) shows an axisymmetric ellipsoid, with a long semi-major axis a and b being the length of the shorter two axes. The last shape is a triaxial ellipsoid, with all three different length axes, represented by a,b and c. The projection of a sphere in the sky will always be a circle. Axisymmetric ellipsoids will have an ellipse as a projection for every angle except one, and the projected shape of a triaxial ellipsoid is always an ellipse. (Source: Wikipedia: Ellipsoid)

1.1.3 Stellar Kinematics

The motion of stars in a galaxy can be quite complex, with highly complicated and chaotic orbits due to the very complex potential of the galaxy. Furthermore, in a dynamically relaxed system, precise information about the stellar motion in the galaxy can tell us the form of its gravitational potential. Knowledge of the gravitational potential can tell us about the mass and matter distributions of the galaxy. Thus, measuring the stellar motion can provide us with a lot of information about the galaxy's dynamical properties.

A set of objects whose motion is used to derive the gravitational potential of a galaxy (or a cluster, in some cases) is called a **kinematic tracer**. While stars are the most prevalent form of tracers because they are bright (and hence easy to observe), common through a large portion of the galaxy and well-understood objects, other tracers also exist and are used by astronomers for a variety of purposes. Gas is another popular type of tracer, which can be used to study some properties that stellar kinematics are not able to properly constrain. For example, due to the presence of extended H-I regions in the outskirts of galaxies, they can be a better tracer to study dark matter, which is thought to be more prevalent in a 'halo' around the luminous portion of the galaxy. Star clusters are also another form of tracer that can be used to probe the gravitational potential. Globular Clusters are found orbiting at the outskirts of the galaxy in the dark matter halos (i.e at very large or eccentric radii) of nearly every galaxy and can serve as excellent tracers for probing the dark matter distribution, and can even be combined with other tracers to get a more detailed dynamical model of the galaxy at small and large radii [12, 13, 14].

But calculating the kinematics of stars is not trivial. The motion of a single star (or any astronomical object) can be broken down into two components. The line of sight motion and the proper motion, which is any motion perpendicular to the line of sight. For the most part, the proper motion of stars can only be determined for stars within the Milky Way, using very high-accuracy photometry. Stars in other galaxies are simply too far for their motion to be perceptible by telescopes. In fact, most external galaxies are too far away for their stars to be individually resolved, making it effectively impossible to observe their proper motions. Only the line of sight kinematics of these stars can be determined.

The line of sight velocity of a single star can be determined using the Doppler Effect. Our knowledge of stellar astrophysics gives us a very good idea of the composition of stars, and also the form of its spectrum in the rest frame. Given the expected wavelength for a particular spectral line expected in stars and the observed wavelength, the line of sight velocity can be calculated by the following formula:

$$\lambda_{obs} = \lambda_{src}\sqrt{\frac{1+v/c}{1-v/c}} \tag{1.1}$$

Where λ_{obs} is the observed wavelength, λ_{src} is the expected wavelength, v is the line

of sight velocity and c is the speed of light.

While this formula gives us the line of sight velocity of a single star, in most cases of observations from external galaxies, the telescope's pixel resolution is simply not high enough to resolve individual stars. Instead, each pixel contains a large number of stars that all move in different directions in general. Thus, we can no longer calculate the exact line of sight velocities of each star, but rather we can estimate certain statistical averages of the motion of these stars, called velocity moments. For example, using 1.1 on the spectrum from a single pixel, we get the mean line of sight velocity(V) instead. Higher moments can also be calculated, which results in the calculation of a probability distribution of line of sight velocities in that particular spatial pixel. This termed as the Line of Sight Velocity Distribution (LOSVD).

1.2 Supermassive Black Holes

Black Holes have historically been highly controversial objects for many scientists, like Einstein. Despite being a prediction from his own theory of General Relativity, he spent many years denying their existence. Evidence for their existence steadily built up over the 20th century, and with recent direct images of black holes at the center of M87 [15] as well as the Milky Way [16], they have become widely accepted as extant objects in the scientific community today.

A black hole is a highly compact object, with its entire mass constrained to be within its Schwarzschild radius ($r_S = \frac{2GM}{c^2}$). Such an object is said to have a singularity at its center, a point of infinite density and gravitational potential. This is surrounded by the event horizon, which is a spherical boundary present at the Schwarzschild Radius inside which it becomes impossible to not fall towards the singularity. The escape velocity at the event horizon is the speed of light, which means it is impossible for anything from the black hole to escape from it, including light itself. General Relativity predicts a plethora of seemingly absurd properties of these exotic objects, but for the purposes of this study, it is sufficient to characterize them as highly compact objects (almost point-like) that emit no light of their own.

There are two broad types of black holes that we observe in the Universe. The first is stellar mass black holes. These black holes have masses on the same order as heavier stars (hence the name), between 5-150 $M_\odot$. Their formation process is relatively well known, being formed after core collapse supernovae of the heaviest stars (any star above the Chandrashekhar Limit) in the universe. The other kind, which is the one we are interested in, are Super-Massive Black Holes (SMBHs). These are found in the centers of nearly every galaxy, and weigh between $10^6 - 10^10 M_\odot$. Their formation is one of the biggest mysteries to modern astrophysics. While earlier theories predicted them to be a result of stellar mass black holes growing by accreting matter over billions of years, recent cosmological simulations and observations of high redshift galaxies cast doubt on this idea [17]. Observed SMBHs are simply too heavy to be formed in this

way. SMBHs, while dark on their own, are responsible for some of the most luminous objects in the universe. Quasars and AGN (Active Galactic Nuclei) are extremely bright galactic cores, caused by a central SMBH accreting a large amount of matter, speeding it up to nearly the speed of light, and giving this accreting matter enough kinetic energy to glow and outshine all the stars in the host galaxy by a large margin.

1.2.1 Measuring Black Hole Masses

There are a few techniques that have been developed over the years to measure the masses of supermassive black holes. The technique used in this work is a specific instance of a broad technique called **dynamical modelling**. The basic principle of the method is as follows: In a gravitationally bound system, the motion of objects in the potential is completely determined by the mass distribution and the position of the object in the system. If the system is dynamically relaxed, the mass distribution is static over suitably large timescales, and the motion of a relatively light object (like a tracer) will not greatly affect it. In other words, given we know the mass distribution of our system (in our case, our galaxy), we can determine the velocities exactly. Conversely, we can reasonably recover the mass distribution if we know the exact velocities of every star in the whole galaxy. If we know the exact mass distribution with high enough accuracy, we can then find the black hole mass by calculating the mass at the galactic center after subtracting the stellar component. Realistically, this is not possible for a number of reasons. Therefore, we must make some simplifications and assumptions to be able to measure the black hole mass using dynamical modelling.

The biggest problem comes from the data and its limited spatial resolution. As mentioned in 1.1.3, for most galaxies, the best we can do is estimate the statistical distribution of the line of sight velocities per pixel, and it is impossible to determine the 3-dimensional velocity vector of each star in it. This means it is no longer possible to solve for the mass distribution in full generality. Instead, we must first make guesses for the mass distribution, solve for the velocity moments, then project this onto the plane of observation, and get a set of model kinematic moments. We keep guessing different forms of the mass distribution until we get model kinematics that are very close to the observations. Of course, it is simply impossible to try every possible mass distribution. To simplify this, we parametrize our mass distribution and change the values of these parameters until we obtain the best-fit model.

Jeans' Anisotropic Modelling (JAM) [18] is one example of a dynamical modelling method. It is majorly used for early-type galaxies, and must assume that they are axisymmetric for the JAM models to be solvable. JAM models the galaxy as a collisionless gas and solves Jeans' Equations to get an analytical description of orbits in the given galaxy's potential. While it has a number of limitations, like only being able to fit the first two kinematic moments, and not being able to use triaxial mass models, it has been shown to be a relatively computationally inexpensive method that is able to constrain parameters like black hole mass and mass-to-light ratio (M/L) fairly accurately and is fairly consistent with other modelling methods for galaxies that it can be used

for. (Importantly, axisymmetric early-type galaxies with constant anisotropy parameter β_z). This technique was also used in [1] to check the consistency between the two types of dynamical modelling.

Schwarzschild modelling [19] is another type of dynamical modelling method and is the one used in this work. It is discussed in detail in 2.5.1.

For galaxies that are further away and not well resolved, dynamical modelling ceases to be an effective tool to measure black hole mass. If the entire galaxy is confined to a single or very few pixels, it becomes impossible to constrain any parameter using dynamical modelling. In fact, if even the Sphere of Influence is not resolved, which is a very tiny fraction of the galaxy's extent, SMBH mass cannot be constrained meaningfully. Instead, we must rely on completely different methods for SMBH mass determination. For high redshift galaxies, we use the spectra of AGN to estimate black hole masses using methods like reverberation mapping [20]. AGN are Supermassive Black Holes accreting a large amount of matter from nearby stars and gas into itself. As this matter falls into the black hole, it accelerates to relativistic speeds, and radiates a large amount of energy, often resulting in the AGN luminosity far exceeding the rest of the galaxy's. AGN also have very distinctive spectra. In particular, they have two types of spectral lines associated with them: Broad emission lines, which come from the accreting material, and Narrow emission lines, which come from the dusty torus of material surrounding the SMBH and accretion disk. The Broad emission lines are related to the rate of accretion of the material, which is in turn related to the mass of the SMBH. Therefore, the mass of the SMBH can hence be calculated. This method fails if the central SMBH is not powering an AGN, or in certain orientations of the AGN, like if the AGN accretion disc is completely edge-on [21].

1.2.2 Black Hole - Host Galaxy Scaling Relations

In order to understand the connection between SMBHs and the galaxies they are present in, astronomers began to look at the relations between the SMBH masses and various properties of the galaxy, including Sersic index(n), bulge velocity dispersion(σ_e), bulge stellar mass and even star formation rates. Surprisingly, even these seemingly unconnected properties showed very tight correlations with the black hole mass[22, 23, 24]. These properties, despite corresponding to vastly different scales, seem to have a very high degree of correlation, which would suggest that these objects evolved together, and actively influence each other through mechanisms that we don't fully understand yet[25, 26]. To get an idea of the difference in scales, a central SMBH is typically less than 1 % of the galaxy's mass, and the sphere of influence, which is the approximate area where the black hole potential dominates the galaxy's potential, is less than a thousandth of the galaxy's luminous extent.

The exact form of the scaling relation is still a matter of debate among astronomers. While earlier studies suggested a single power law [25], more recent research points towards more complex models, like a double power law [27] or a three parameter plane

[28] to properly quantify the scaling relation. Recent studies have also shown that the low and high mass regimes also have an upward deviation from the expected trend [29], which casts doubt on the existence of a universal scaling relation. More SMBH mass measurements would hence be needed, using various and independent methods to be able to better constrain the true nature of the scaling relations. More observations of the low and high ends of the relation will also help reduce the systematic uncertainties and the high intrinsic scatter at those ranges, helping us better understand the mechanism behind SMBH-galaxy co-evolution. These would also help us understand if the scatter observed in the scaling relations is due to observational uncertainties or due to a physical process.

1.3 Dark Matter

When astronomers were looking at the rotation curves of galaxies (that is, the plot of the rotational velocity of the galaxy vs distance from the center), they noticed an anomaly. The rotation curve could not be explained by the matter present in the galaxy. The difference between the expected rotation curve and the real observed rotation was significant, and more importantly, it showed the same pattern across multiple galaxies, including our own. The most plausible explanation at that time seemed to be that some form of matter that had mass but did not interact with light surrounded nearly every galaxy. While this additional 'dark matter' term could explain the rotation curves, calculating the total mass of this dark matter would result in a mass much greater than the mass of the ordinary matter of the galaxy. Thus, the idea of a mysterious form of matter called dark matter was born. Even now, astronomers and physicists do not fully understand its physical nature.

Currently, the most popular cosmological model is the ΛCDM model. The Λ stands for the vacuum energy constant from general relativity, while CDM stands for Cold Dark Matter. Modern astronomers believe that the energy content of the universe is dominated by two poorly understood phenomena: Dark energy (which makes up about 70% of the universe's energy), which is responsible for the accelerated expansion of the universe, and dark matter (which is about 20% of the universe's energy content), which is responsible for the formation of large scale structures like galaxies and galaxy clusters. Baryonic matter, which is matter made of atoms and molecules, only makes up 5% of the universe's energy content. ΛCDM expands on this by modelling dark energy expansion as a consequence of a positive vacuum energy constant and modelling dark matter as a dynamically cold substance (that is, there is little to no random motion in the dark matter particles). While ΛCDM has successfully explained many phenomena, it is still a phenomenological model that provides no explanation of the origin or nature of dark matter and energy. It also has failed to explain some phenomena, leading to it (and more specifically improving it) becoming an active area of research.

ΛCDM predicts that large-scale structures are born from small adiabatic fluctuations in the very early universe, prior to recombination. As the universe expanded, the energy

density of the universe began to reduce, leading to recombination and photons decoupling from baryons. This led to the Cosmic Microwave Background, which was released when recombination ended. One of the biggest successes of ΛCDM comes from its highly accurate prediction of the CMB power spectrum, which relates the length scales of the anisotropy to the frequency with which they occur. These anisotropies, enhanced by the force of gravity, grew into the large scale structures like galaxies and galaxy clusters that we see today [30, 31]. ΛCDM also predicts the existence and number density of galactic scale halos fairly accurately.

Despite its successes, it still has a number of shortcomings and phenomena it is unable to account for or has a number of predictions that have not been observed. The first is the missing satellites problem [30]. CDM predicts that subhalos of all length/mass scales exist, and as the size of the halo decreases, the number of halos of that size should increase. However, this increase in frequency and the presence of such halos are not observed. For example, the number of observed satellite dwarf galaxies orbiting the Milky Way is much lower than the number predicted by the model. We see ≈ 400 satellites of $\geq 200 M_{\odot}$, while we estimate it to be more than 10^5! There are possible resolutions to this discrepancy, the most popular of which being that these subhalos exist, but are simply too inefficient at capturing enough material to start star formation, or are almost completely devoid of any baryonic matter [30]. The second is the excess mass at the cores [30]. Almost all types of halo profiles predicted by CDM predict a central dark matter concentration which is much higher than what is observed. This can be verified by observing the rotation curves, which are much shallower in observed galaxies than the ones predicted by CDM simulations. Additionally, the total mass of the dark halo is predicted to be much higher than what is observed. A more detailed look at the properties and problems related to Λ CDM can be seen in [30].

1.4 Aims of the project

This project studies how a more generalized model of the galaxy affects the SMBH mass measurement using Schwarzschild Modelling. More specifically, [1] was a study that looked at a sample of six galaxies and measured their respective central black holes. However, several strong assumptions were made, that might not necessarily hold for this sample. Firstly, the galaxies were assumed to be axisymmetric, which is not true for early-type galaxies in general. Secondly, the effect of dark matter was completely ignored. This was a very strong assumption, as we know that every galaxy is embedded in a dark matter halo. While there is an argument to be made that the dark matter halo will not greatly affect the SMBH mass measurement, due to it not affecting the central region of the galaxy significantly, this has not been fully verified before. This work relaxes these assumptions, allowing for a fully triaxial galaxy shape and including (relatively simple) dark matter models and studies how including this and making a more complex overall model affects this measurement. Additionally, it also provides a consistency check between DYNAMITE [32, 33], a routine developed at the University of Vienna that can do triaxial Schwarzschild modelling and other routines that perform

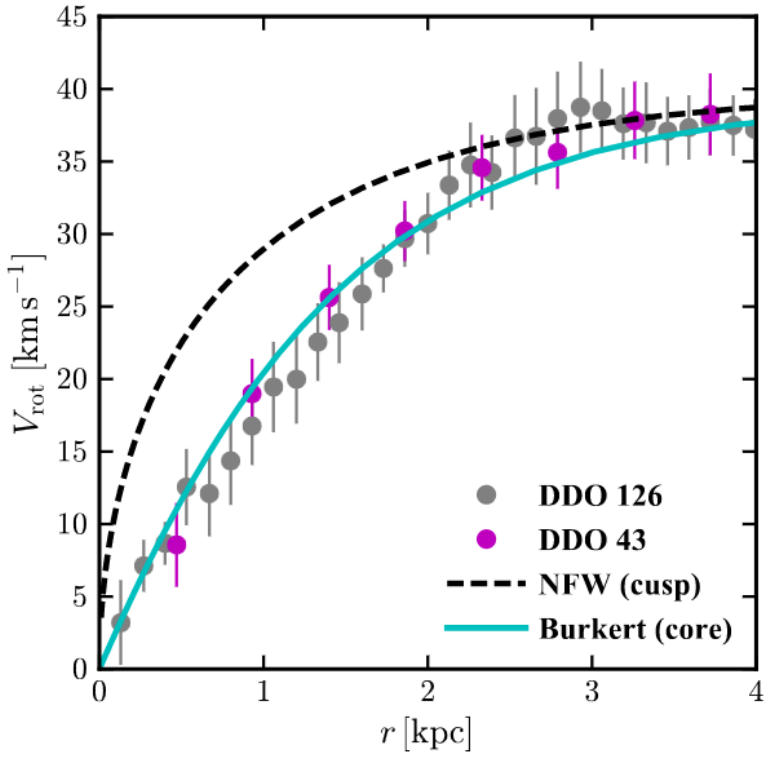

Figure 1.4: This figure demonstrates the core-cusp problem present in CDM. NFW (black dashed line) is a type of halo profile consistent with ΛCDM. The lines are from dark matter-only simulations, with NFW being the prediction by Λ CDM and the Burkert model having a constant density core being a correction to the NFW halo profile to account for data (represented by points). As we can see, for multiple galaxies, NFW (or CDM) consistently predicts a shallower rotation curve. Plot is taken from [30]

axisymmetric Schwarzschild modelling.

Chapter 2

Methods

2.1 Sample

In this work, three galaxies from the SMASHING sample were selected, the dynamics of which were studied in [1]. This was done so that this analysis would serve as a comparison study between axisymmetric dynamical models without the effect of dark matter (used in [1]) and triaxial dynamical models incorporating dark matter models.

The SMASHING sample was created to use 8m ground-based telescopes to fill up gaps in the data for scaling relations for early-type galaxies. It consists of 19 galaxies and is further explored in [34, 1, 35]. The observations made use of Adaptive Optics (AO) technology, made possible by Natural Guide Stars (NGS) and Laser Guide Stars (LGS). At the time of its creation in 2009, most SMBH mass measurements had come from HST data (except for [36] and [37]). The SMASHING sample aimed to extend the methodology in [36] and [37] to a wide range of early-type galaxies using ground-based spectroscopy combined with NGS and LGS AO. AO to adjust for disturbances from the atmosphere that causes blurry images in ground-based telescopes. AO helps mitigate that by actively adjusting for changes in the atmosphere's refractive index and other optical properties, allowing ground based telescopes to achieve a much higher resolution.

Unlike previous works in determining SMBH mass, this work, along with [1], combines high spatial resolution of the galactic centers using INtegral Field Observations using the Near Infrared spectrograph (SINFONI) to resolve the black hole's Sphere of Influence(SoI), with large scale data to better probe stars at large elliptical radii and better constrain the global stellar mass to light ratio (M/L). The radius of the black hole's sphere of influence is given by:

$$r_{SoI} = \frac{GM_{BH}}{\sigma^2} \tag{2.1}$$

Where M_{BH} is the mass of the black hole, which can be estimated from previous scaling relations to get an estimate of r_{SoI}, and σ is the velocity dispersion of the galaxy. The SoI is the region around the central black hole where the gravitational potential due

Name	Type	Distance (Mpc)	Large scale data source	Stellar Mass ($M_\odot$)
NGC 584	S0	19.1 ± 1.0	MUSE	1.0×10^{11}
NGC 4281	S0	24.4 ± 2.2	SAURON	5.8×10^{10}
NGC 4570	S0	17.1 ± 1.3	SAURON	1.6×10^{11}

Table 2.1: This table gives some details of the galaxies studied in this work. All high resolution datasets are from the SINFONI IFU. Morphological types and distances are taken from [1]. The Mass column indicates the total stellar mass and is taken from [38].

to the SMBH dominates all the other sources of gravity. The details of the galaxies used in this study are given below:

2.2 Observations

Each galaxy analyzed in this work has a set of two datasets. The high-resolution data of the center is observed for each galaxy by SINFONI, an instrument mounted on UT4 of the Very Large Telescope (VLT) at Cerro Paranal, Chile. SINFONI as an instrument consists of the Spectrometer for Infrared Faint Field Imaging (SPIFFI) and the Adaptive Optics module, Multi-Application Curvature Adaptive Optics (MACAO). The observations were done between 2007 and 2013, in the K-band grating (1.94-2.45 μm) with a spectral resolution of R $\sim$ 4000 and a pixel scale of 100 mas. The total field of view per pointing hence was 3.2" $\times$ 3.2".

The large-scale data for our sample comes from two different sources. The Multi Unit Spectroscopic Explorer (MUSE) IFU, another instrument on the VLT, was used for NGC 584. For NGC 4281 and NGC 4570, the Spectrographic Areal Unit for Research on Optical Nebulae (SAURON) IFU was used, which is mounted on the William Herschel Telescope at the observatorio del Roque de los Muchachos on La Palma. These two galaxies were also part of the ATLAS 3D survey [38]. MUSE has a field of view of 60" $\times$ 60", with one pixel being 0.2" $\times$ 0.2". SAURON has a field of view of 33" $\times$ 41", with 0.94" $\times$ 0.94" square pixels.

2.3 Extraction of Stellar Kinematics

In order to make accurate dynamical models of galaxies to measure the mass of the central black hole, high-quality data of the kinematics, that is, the information about the motion of stars is needed. Since the instruments used in this work cannot resolve individual stars in galaxies that are not the Milky Way such as those in the SMASHING galaxy sample, we seek to extract the statistical properties of their motion instead.

To understand how these stars move in the galaxy, we must discern this information from the light they emit. More specifically, we use the galaxy's spectra (For example, see Figure 2.3). The basic principle is as follows: Observing nearby stars in the Milky Way allows us to see their spectra in great detail, and allows us to determine the precise

form of their spectral lines and continuum in the rest frame. More precisely, we can observe very detailed spectra of Milky Way stars and use those as a 'stellar template' to compare our observations to. Since the stars in our target galaxies have some motion relative to us, the shift and spread in their spectral lines compared to the rest frame lines, which we know from our stellar template. The Doppler Effect gives us the relation between the shift in the spectral line and the velocity of the light source (in our case, stars) along the line of sight. However, since each pixel contains a multitude of stars, only the statistical moments of velocity along the line of sight can be calculated. Without accurate knowledge of proper motions (motion perpendicular to the line of sight), there is no way to obtain the true velocity moments. The total statistical distribution of the line of sight velocities of stars in a single pixel (or bin) is called the Line Of Sight Velocity Distribution (LOSVD).

In this analysis, we study the first four moments of the LOSVD, which we parametrize using a Gauss-Hermite polynomial. The first moment is the mean velocity (V), the second is the velocity dispersion (σ), and the third and fourth give the asymmetric deviations/skew (h_3) and the symmetric deviations/kurtosis (h_4) respectively. The form for our Gauss-Hermite polynomial is given by:

$$\mathscr{L}(y) = \frac{exp(-y^2/2)}{\sigma\sqrt{2\pi}}[1 + \sum_{m=3}^{M} h_m H_m(y)] \tag{2.2}$$

Where $y = \frac{v-V}{\sigma}$ and $H_m(y)$ are Hermite polynomials of order 'm'. For our purposes, we set M=4 to obtain our four kinematic moments, V, σ, h_3 and h_4. Here, we have implicitly set h_0 to 1 and h_1 and h_2 to 0 because we want to maintain Orthogonality between all the terms but also not include redundant parameters (h_1 is also a measure of the central tendency like the mean and h_2 is also related to the variance of the distribution).

The LOSVD is derived by comparing our observed spectra to known stellar templates, giving us a complete probability distribution of velocities along the line of sight. A Gauss-Hermite polynomial is then fitted to this LOSVD, and we get values for each fitted kinematic moment for that pixel (or bin).

2.3.1 Voronoi Binning

Before we derive the stellar kinematics from the spectra, we must first bin pixels in the datacube, to ensure that we do not fit to any noise. Since spectral fitting corresponds to fitting to sharp and very precise peaks, it is extremely sensitive to noise. Any spurious fluctuations due to the atmosphere, interstellar gas or a similar source can lead to very bad fits. To ensure a standard baseline for noise, we must bin multiple pixels together and co-add their spectra to ensure a sufficiently high Signal-to-noise ratio (S/N), enough to fit to stellar spectral lines reasonably accurately.

Voronoi Binning [39] is a method that produces bins that ensure a minimum target S/N (which is an input set by us). It also has the added constraint of making approxi-

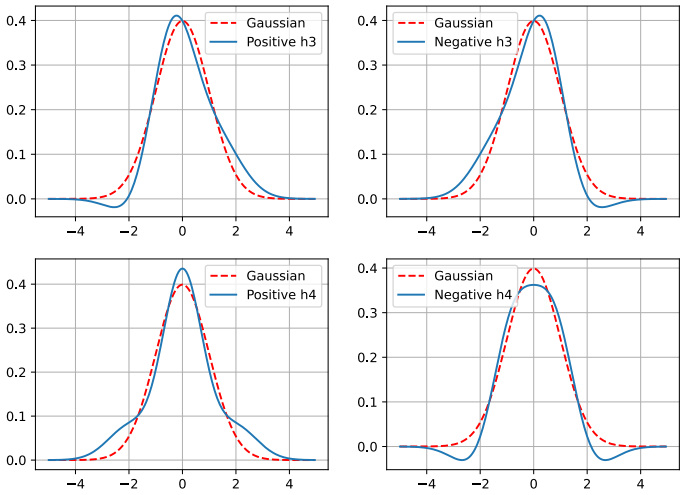

Figure 2.1: These plots show how the inclusion of the Hermite polynomials influence the Gaussian. A positive h_3 introduces a rightward skew, and a negative h_3 introduces a leftward skew. A positive h_4 gives the gaussian a narrower peak and thicker tails, while a negative h_4 does the opposite.

mately round bins. In this work, the target S/N was set to a value between 40 and 70, depending on the galaxy. This is chosen so that we have unbinned spatial pixels (spaxels) at the galactic center to ensure the highest possible spatial resolution for SMBH mass determination while keeping high S/N at the edges of the image to ensure a good fit. The benefit of this binning method is that it decreases the relative error (which is the same as improving S/N) for outer bins.

2.3.2 Penalized PiXel Fitting (pPXF)

A standard library to extract kinematics is penalized Pixel Fitting (pPXF) [40][41]. pPXF takes the binned spectra as an input, fits a standard stellar template to the observed binned spectra and gives kinematic maps of the first four moments of the LOSVD. A stellar template is the rest frame spectrum of a certain type of star we expect to see in the galaxy. A stellar template library consists of a large number of such spectra, which can be used to comprehensively estimate the stellar populations in the galaxy. For this study, we use the MILES stellar template library [42] for MUSE and ATLAS data, while using the stellar template library created in [43] for SINFONI.

The first step in the Penalized Pixel Fitting process is extracting the LOSVD from the spectra of each bin. A model galaxy spectrum is constructed, which consists of a weighted sum of stellar templates, with added weighted polynomials which account for bad sky regions and atmospheric corrections. Furthermore, the stellar template is convolved with the LOSVD [44, 41]. pPXF fits each bin to a model galaxy spectrum (see full equation below) using regularized non-negative least squares fitting to ob-

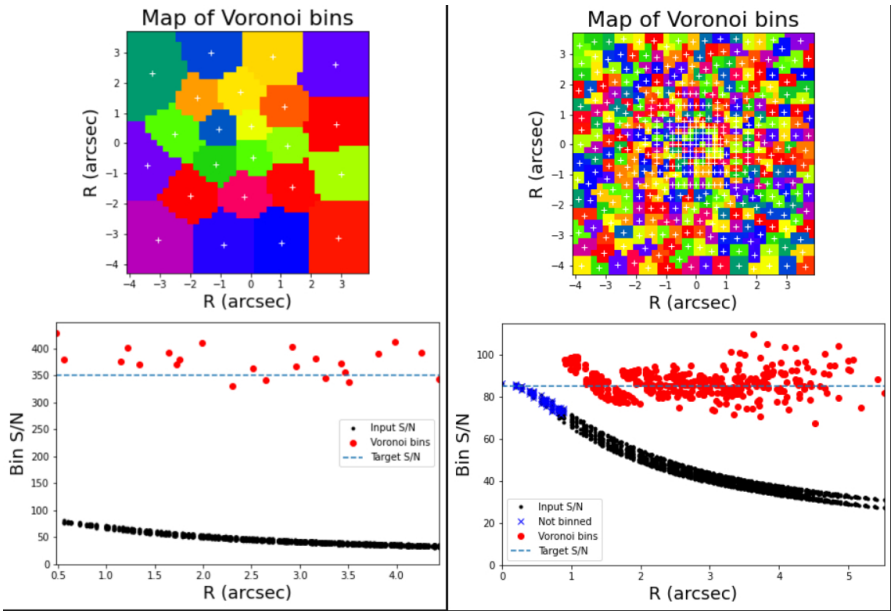

Figure 2.2: This figure shows Voronoi Binning done for two different values of S/N. The two figures on the left depict the binning procedure for NGC584 for S/N = 350, while the right depicts S/N = 85. The upper row depicts the unbinned and binned S/N and the bottom row depicts the bins on the image.

tain the weights. Then, adopting a standard truncated Gauss-Hermite expansion as a parametrization for the LOSVD [44], it finds the best fit for each of the Gauss-Hermite coefficients. As mentioned before, we fit for the first four coefficients: V, σ, h_3, h_4. Mathematically, we have the model galaxy spectrum ($G_{mod}(x)$) given by:

$$G_{mod}(x) = \sum_{n=1}^{N} w_n\{[T_n(x) * \mathscr{L}_n(cx)] \sum_{k=1}^{K} a_k \mathscr{P}_k(x)\} + \sum_{l=0}^{L} b_l \mathscr{P}_l(x) + \sum_{j=1}^{J} c_j \mathscr{S}_j(x) \quad (2.3)$$

Here,$x = ln(\lambda)$, where λ is the wavelength. $T_n(x)$ is a stellar template, N denotes the number of templates in the stellar template library, $\mathscr{L}_n(cx)$ is the LOSVD, $*$ symbolizes convolution, $\mathscr{S}_j(x)$ are sky spectra, $\mathscr{P}_k(x)$ are multiplicative orthogonal polynomials of degree 'k' that account for inaccuracies in spectral calibration and reduce the sensitivity to dust reddening and $\mathscr{P}_l(x)$ are additive orthogonal polynomials of degree 'l' that account for template mismatch, sky correction and scattering due to the sky [41].

The residuals (for a single good pixel) are then defined as:

$$r_n = \frac{G_{mod}(x_n) - G(x_n)}{\Delta G(x_n)} \quad (2.4)$$

Where $G(x_n)$ is the observed galaxy spectrum and $\Delta G(x_n)$ is the observational error. The chi-squared to be minimized is therefore:

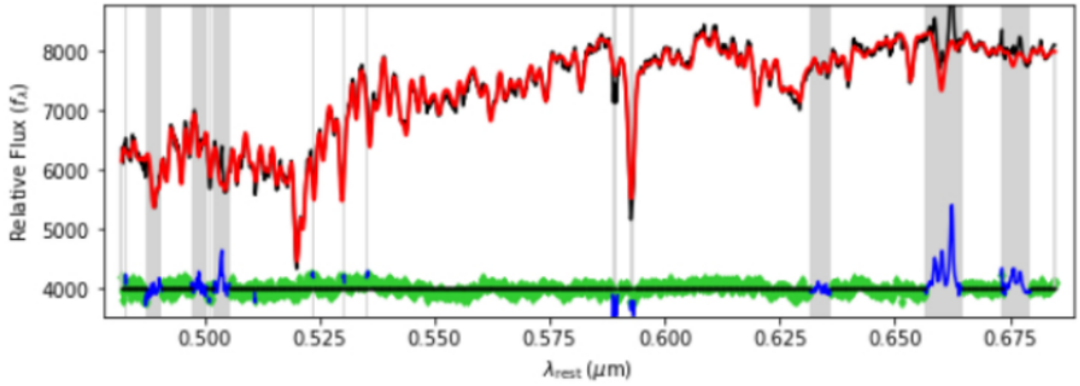

Figure 2.3: This figure shows a pPXF fit for a single bin. The black line represents the observed spectrum, while the red line represents the pPXF fit. The grey region shows masked regions where the algorithm identifies sources of error like atmospheric absorption. The green line shows the residuals shifted up to 4000 (for ease of viewing), while the blue line shows the residuals of the masked regions.

$$\chi^2_P = \sum_{n=1} N r_n^2 + \alpha \mathscr{P} \tag{2.5}$$

Where N is the number of good pixels and the second term is the regularization factor. (see [41] for details on the fitting procedure.)

In accordance with the standard LOSVD parametrization as a truncated Gauss-Hermite expansion, we fit it to equation 2.2.

An example of a pPXF fit can be seen in Figure 2.3

Finally, now that we have kinematic maps for each of the moments from pPXF, these serve as the input data that our dynamical models will try to fit to.

2.3.3 Comparison of Kinematic Datasets

A further step to ensure the consistency of the high-resolution and large-scale datacubes is to verify the radial profiles of the four kinematic moments match. This preliminary step helps us eliminate systematic uncertainties that may cause problems in dynamical modelling. In order to make a comparison, however, it is not as simple as comparing the profile of a particular moment along the major axis. Since the large-scale data and the high-resolution SINFONI data have different Point Spread Functions (PSFs), it is important to convolve the high-resolution data (which has a narrower PSF) with the effective PSF to make a valid profile comparison.

Assuming the PSFs are Gaussian, the Full Width Half Maxima (FWHM) can be found in the header file in the datacube. The standard deviation of the Gaussian PSF can therefore be calculated using the simple relation:

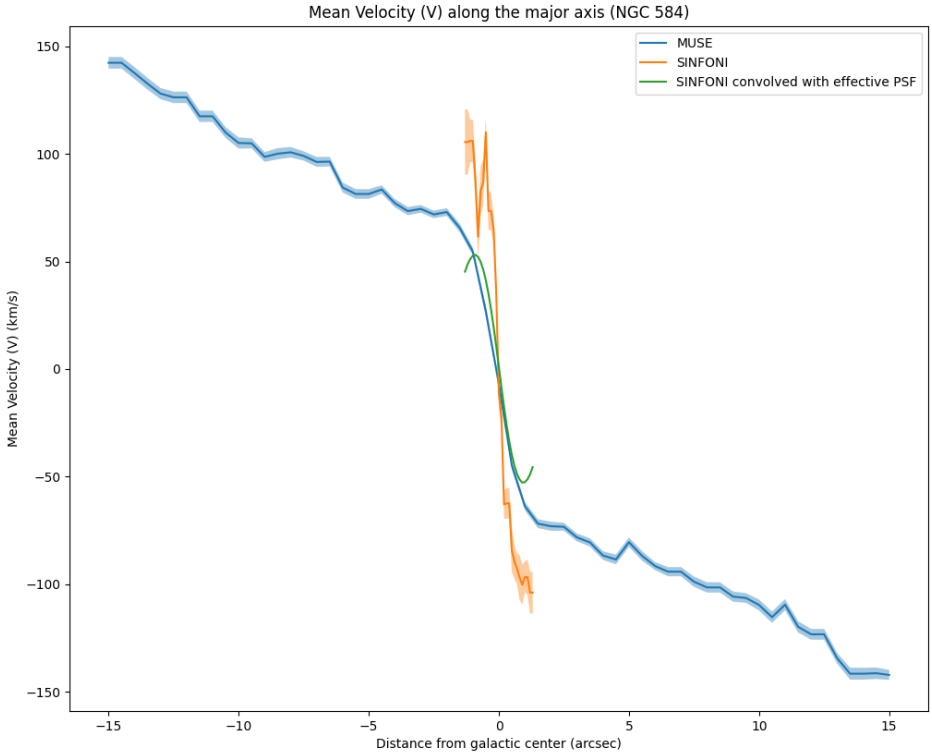

Figure 2.4: This plot shows the Mean Velocity of the pixels along the major axis of NGC 584. The blue line is the velocity profile from the large-scale data (MUSE) and the orange line is the velocity profile for the high-resolution SINFONI data. The shaded regions show the uncertainties for each velocity profile. The green curve is the convolution of the SINFONI profile with the effective PSF. As we can see, the slopes of the convolution and the MUSE velocity profile are consistent. The curved ends of the convolved velocity profile is due to the finiteness of the SINFONI velocity profile.

$$FWHM = 2\sqrt{2ln(2)}\sigma \approx 2.355\sigma \tag{2.6}$$

Then, the standard deviation of the effective PSF is given by:

$$\sigma^2_{eff} = \sigma^2_{LS} - \sigma^2_{SINFONI} \tag{2.7}$$

The transformed radial profile (from SINFONI data) of a particular kinematic moment is therefore given by:

$$f_{conv}(r) = f(r) * \frac{1}{\sigma\sqrt{2\pi}} exp(-\frac{r^2}{2\sigma^2}) \tag{2.8}$$

This profile can now be compared to the profile from the large-scale data to check for consistency. For NGC 584, the velocity dispersion profiles along the major axis were found to be slightly shifted from each other, so these were manually adjusted to make them match. The plot in 2.4 shows the mean LOS velocity along the major axes for both galaxies.

2.4 Finding the Stellar Potential

The total gravitational potential in the galaxy can be written as:

$$\Phi_{tot} = \Phi_{star} + \Phi_{SMBH} + \Phi_{DM} \tag{2.9}$$

Finding the gravitational potential due to the Black Hole will also allow us to calculate its mass. The potentials due to the Dark Matter and the SMBH, however, can only be reasonably calculated with dynamical modelling. The total gravitational potential is what dictates the kinematics that we observe and can be inferred from it. The easiest component to calculate is the mass distribution (and therefore the potential) due to the stars as they are directly observed by the telescopes, as well as being far more well understood.

High-resolution images of the galaxies help us create a very accurate map of the surface brightness of the galaxy. Modelling this surface brightness, and then multiplying it with a characteristic scalar Mass-to-Light ratio will give us the mass model for the stars. In order to model the surface brightness, we parameterize it using Multi-Gaussian Expansion (MGE) [1].

2.4.1 Multi-Gaussian Expansion(MGE)

The Multi-Gaussian Expansion (MGE) is a method to model the surface brightness of a galaxy [45]. It models the surface luminosity as a sum of concentric, two-dimensional Gaussians, centered at the center of the galaxy. These are fit using a python library called 'MGEfit'. Very high-resolution HST images are used for MGE fitting, to get the most accurate light model [1].

Mathematically, we start with the PSF (in our case, the PSF of the HST). Assuming it can be written as a sum of (2-D) Gaussians, we write:

$$PSF(x',y') = \sum_{k=0}^{m} G'_{*k} \tag{2.10}$$

With G'_{*k} defined as:

$$G'_{*k} = I'_{*k} exp\{-\frac{1}{2\sigma'^2_{*k}}(x'^2_{*k} + \frac{y'^2_{*k}}{q'^2_{*k}})\} \tag{2.11}$$

With

$$x'_{*k} = (x' - x'_{0*k})cos(\alpha'_{*k}) + (y' - y'_{0*k})sin(\alpha'_{*k}) \tag{2.12}$$

$$y'_{*k} = -(x' - x'_{0*k})sin(\alpha'_{*k}) + (y' - y'_{0*k})cos(\alpha'_{*k}) \tag{2.13}$$

Here, σ_{*k} represents the standard deviation of the kth Gaussian and q_{*k} represents its axial ratio. (x'_{0*k}, y'_{0*k}) represents the Cartesian coordinates of the point of maximum intensity or center, while I'_{*k} represents the maximum intensity. Finally, α'_{*k} represents the position angle of the major axis of the Gaussian.

The deconvolved surface brightness $\nu'(x',y')$ is given by:

$$\nu'(x',y') = \sum_{i=0}^{N} G'_i = \sum_{i=0}^{N} I'_i exp\{-\frac{1}{2\sigma'^2_i}(x'^2_i + \frac{y'^2_i}{q'^2_i})\} \tag{2.14}$$

With

$$x'_i = (x' - x'_{0i})cos(\beta_i) + (y' - y'_{0i})sin(\beta_i) \tag{2.15}$$

$$y'_i = -(x' - x'_{0i})sin(\beta_i) + (y' - y'_{0i})cos(\beta_i) \tag{2.16}$$

Therefore, the convolved surface brightness becomes:

$$\rho(x',y') = \nu' \otimes PSF = \sum_i G'_i \otimes \sum_k G'_k = \sum_{i,k}(G'_i \otimes G'_k) = \sum_{i,k} G'_{i,k} \tag{2.17}$$

Which is also a sum of Gaussians. The MGEs are hence fitted to the observed surface brightness profiles using ordinary least squares with a set fixed number of Gaussians, usually somewhere between 10 and 12. An example MGE fit is shown in Figure 2.5.

The next step to extract the 3-dimensional stellar potential is MGE deprojection. Deprojection gives us a 3-D Luminosity distribution that is, in general, non-unique [45]. However, certain conditions are necessary for the deprojection to be possible. Firstly, a certain shape has to be assumed about the Luminosity distribution. In this study, it is assumed to be a triaxial ellipsoid (see Figure 1.3) . This differs from [1], where the underlying distribution was assumed to be axisymmetric. The second condition is

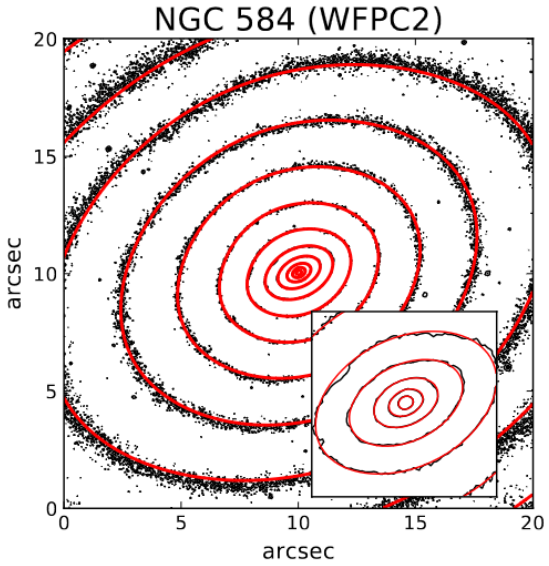

Figure 2.5: This figure depicts an MGE fitted to NGC584. The black lines are isophotal contours of the HST data while the red lines depict contours of the fitted MGE. Taken from [1].

that the inclination angle, i, must be within a range of values for deprojection to be meaningfully done. For example, if the galaxy is edge-on, the plane of the galaxy is completely obscured from us, and the true 3-D distribution cannot be found. Therefore, for low inclination angles, the uncertainties in the deprojection become very large and the resultant 3-D deprojection becomes unreliable. An inclination angle of 40^o to about 85^o is preferred for deprojection.

In this study, the MGEs used for each sample galaxy is the same as the ones used in [1], as they are the same galaxy, and using the same MGE will ensure more consistency in results and less sources of difference. However, due to different shape assumptions, the method of deprojection are different. Since for each dynamical model, we also vary the shape parameters and hence we must deproject the MGE again. Therefore the deprojection is done by the dynamical modelling software, which in our case is the DYNamics, Age and Metallicity Indicators Tracing Evolution (DYNAMITE) software developed at the University of Vienna. [32] [33]. The details of the procedure is explained in the next section, while the specifics of DYNAMITE is explained in section 2.5.2. The MGE is therefore the first input we must give to DYNAMITE for it to be able to do dynamical modelling.

2.5 Dynamical Modelling

In order to constrain the other two components (Black Hole and Dark Matter) of the galactic potential, we must perform dynamical modelling of the galaxy and fit it to the observed kinematics. In other words, a certain model potential is taken, and various

stellar orbits are calculated in this potential, with different weights assigned to each orbit that are fitted to the observed kinematics to provide the closest approximation/best-fitting model. This process is repeated by changing the potential by way of changing one or more parameters until the best possible model is obtained. This, in simple terms, is the core of orbit superposition methods.

2.5.1 Schwarzschild Method

The Schwarzschild method of dynamical modelling [19] is used in this study to measure SMBH masses. Further works like [46] modified it to fit stellar kinematics and [47] expanded it to ellipticals and attempted to model dark matter halos as well. The general assumption throughout the Schwarzschild method is that the object in question is in dynamical equilibrium. In order to find the right SMBH mass, we must repeat the modelling process a large number of times and find the one that most closely reproduces the observed kinematics. This method also assumes that the potential due to the various components is stationary, which is fairly accurate for dynamically relaxed systems at large length and time scales. The general procedure of Schwarzschild modelling is:

First, assuming a stationary potential, a representative orbit library is constructed. An orbit library is a list of model stars that have differing initial conditions and are made to go around the constructed potential. There are three integrals of motion that determine a stellar orbit. First is the total mechanical energy (E) along with two non-classical (here, non-classical signifies that it does not hold any physical meaning) integrals (I_2 and I_3). For each combination of these values, a stable orbit in the given fixed potential exists. Each orbit is traced by a test particle for 200 periods to get a representative characteristic of each orbit in equilibrium for the galaxy. In a triaxial potential, there are four main types of orbits, which arise at different combinations of the three integrals. Box orbits (so called because they cover a 2-D surface reminiscent of a box) and short, middle and long-axis tube orbits (they are constrained to be within a tube-shaped boundary of differing shapes depending on the orbit family).

In the second step, all orbits are projected onto the plane of the observables and made to match the LOSVD as well as the observed flux map. Each orbit is assigned a weight which are the parameters used to fit to the LOSVD, using Non Negative Linear Squares (NNLS) fitting. The best fit for the current potential is thus found.

This process is then repeated for each guess of our potential in our permitted parameter space. Each component of the galactic potential has a different parametrization, and thus, depending on their forms and number of free parameters can greatly affect the time complexity of the problem. The exact nature of the parametrizations used here are discussed in section 2.5.2. In general, Schwarzschild modelling is able to encode a large variety of models of the galactic potential, but constraining individual parameters becomes difficult the more parameters there are. In addition, since each iteration of the dynamical modelling algorithm involves the deprojection of the mass model, calculation of the total potential, tracing the orbits for a large library (typically containing

more than 100,000 stars) and doing an NNLS fit of these large number of orbit weights, it is fairly computationally intensive. As such, simpler models for the various galaxy components (especially the dark matter halo) are preferred.

2.5.2 DYNAMITE

DYNamics, Age and Metallicity Indicators Tracing Evolution (DYNAMITE) is a tool developed at the University of Vienna to study a number of galaxy properties that give insight into its structure and history. It has been used in this work extensively to perform triaxial Schwarzschild modelling [33, 32, 9].

An important step before we start modelling is data preparation. This converts the stellar kinematics extracted by pPXF to a form that is readable by the software. The `create_kin_input` routine reads the FITS tables that contain the binned kinematics and gives three files as output: `bins.dat`,`aperture.dat` and `gauss_hermite_kins.ecsv`. These files contain the same information as the FITS tables but in a format that DYNAMITE can read, in addition to the corresponding PSF. The data preparation also fits the position angle, which is the angle between the vertical and the axis of rotation. The rotational major axis of the galaxy is the line perpendicular to this line and is the line along which the maximal line of sight rotation is observed. An example of the position angle fit is given in 2.6.

In order to perform dynamical modelling, DYNAMITE requires several inputs. These are:

1. The fitted MGE, which describes the light model for the galaxy.
2. The observed kinematic data with the kinematic maps of each Gauss-Hermite moment for both the large-scale and high-resolution data.
3. The PSFs for both the large-scale and high-resolution data.
4. A grid of allowed parameter values for each free parameter present in the total galactic potential.

The MGE is obtained from the MGEfit routine described in the previous section. The observed kinematics and Gauss-Hermite moment maps are obtained from the pPXF routine fitting. The allowed parameter values and free parameters are given by us for each run of the DYNAMITE code, changed in between runs to efficiently but thoroughly search the parameter space for the best fitting model. As discussed above, there are a variety of parametrizations possible for each component of the potential. The specific parametrizations used are discussed below.

The stellar potential: The potential due to the stars is described by the MGE, as discussed above. DYNAMITE performs deprojection on the MGE to get a 3-dimensional

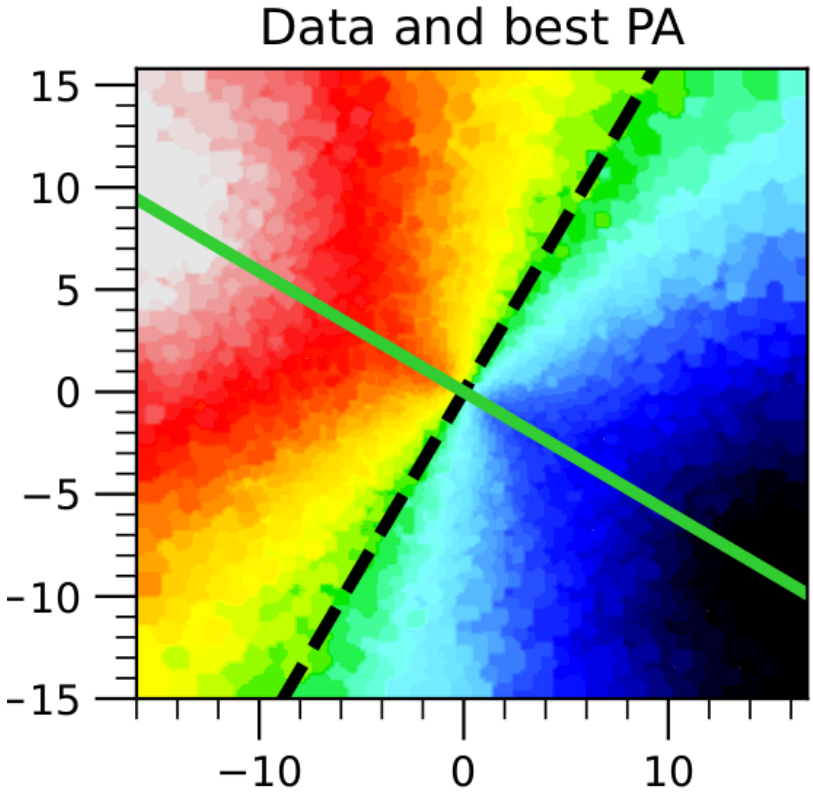

Figure 2.6: This figure shows the fitted position angle for NGC 584. The kinematic map shown is the mean velocity per pixel (V) for the large-scale MUSE data for NGC 584. The dashed black line shows the axis of rotation, while the solid green line perpendicular to it is called the kinematic major axis.

distribution of stellar luminosity throughout the galaxy (if the angle of inclination is appropriate for deprojection). Since we work with triaxial shapes, we have three parameters constraining the shape of the galaxy, p, q and u. These are the shape parameters, with their relations to the axis lengths of the ellipsoid given below:

$$p = b/a \tag{2.18}$$

$$q = c/a \tag{2.19}$$

$$u = \sigma'/\sigma \tag{2.20}$$

Where a, b and c are the half-axis lengths of the ellipsoid with $a \geq b \geq c$ (see Figure 1.3 for visual representation of a,b and c). σ' denotes the deviation of the Gaussian projected in the plane of observation while σ is the deviation of the intrinsic 3-D distribution. u is also sometimes called the compression factor.

The last parameter is the mass-to-light ratio M/L. This parameter is multiplied with the deprojected MGE to recover the mass distribution of the stars in the galaxy. In our study, we use a constant M/L, that is, it is a constant scalar independent of location in the galaxy. While studies have shown that the assumption of a constant M/L is often inadequate to properly describe the mass distributions of stars [48], it does not greatly affect the SMBH mass measurement, while also staying consistent to [1], which also uses constant M/L.

The Black Hole Potential: The potential due to the SMBH is parametrized as a Plummer black hole, with mass M and softening length a, given by:

$$\Phi_{BH}(x,y,z) = -\frac{GM}{\sqrt{x^2+y^2+z^2+a^2}} \tag{2.21}$$

This is the standard potential due to a point mass with a small additive factor in the form of the softening length. This is done to avoid infinities in the computation very close to the black hole.

The Dark Matter Potential: The potential due to the Dark Matter halo is parametrized as a spherical Navarro-Frenk-White (NFW) halo with two parameters, the mass fraction f and the dark matter concentration c. The density profile of the NFW halo is given by:

$$\rho_{DM}(r) = \frac{\rho_0}{\frac{r}{R_s}(1+\frac{r}{R_s})^2} \tag{2.22}$$

Where R_s is the scale radius. The potential is hence given by:

$$\Phi_{DM}(r) = -\frac{4\pi G\rho_0 R_s^3}{r} ln(1+\frac{r}{R_s}) \tag{2.23}$$

Here are two parameters become the scale radius R_s and ρ_0. But instead of these, we prefer to use the concentration parameter, c, and the fraction of dark matter within

the virial radius, f. They are defined as:

$$c = \frac{R_{200}}{R_s} \tag{2.24}$$

$$f = \frac{M_{200}}{M_*} \tag{2.25}$$

Where R_{200} is the virial radius, M_{200} is the total Dark Matter mass inside the virial radius and M_* is the total stellar mass. Therefore, in terms of the original parameters, they can be written as:

$$\rho_0 = \frac{200}{3} \frac{c^3}{ln(1+c) - \frac{c}{1+c}} \rho_{crit} \tag{2.26}$$

$$R_s = [\frac{3}{100\pi} \frac{M_* f}{\rho_{crit} c^3}]^{1/3} \tag{2.27}$$

To further simplify our models, we can eliminate c as a free parameter and just use the dark matter fraction f instead. [49] gives a way to write c in terms of f for the NFW halo of an elliptical galaxy, provided the redshift is known. This relation is given by:

$$log_{10}(c) = 0.905 - 0.101 log_{10}(\frac{M_{200}}{[10^{12} h^{-1} M_\odot]}) \tag{2.28}$$

All of these parameters are specified in the config file of DYNAMITE. The config file also specifies which parameters are free to be varied by the modelling software, as well as what possible values they could take. Since dynamical modelling is extremely computationally intensive, setting all parameters free across a large set of parameters will take extremely long to compute. Therefore, it is necessary to only keep certain parameters free for a particular run and run multiple such runs (with different parameters kept free) to eventually converge to the best possible model.

There are also two modes of exploring the available parameter space that can be used for slightly different functions. While both modes try to fit by minimizing the same function (kinematic χ^2), the method of iterating between different models changes. `LegacyGridSearch` is a more efficient algorithm, checking nearby values in parameter space and stopping if moving in that direction yields a very high kinematic χ^2. While efficient, there is always a chance that this mode falls into a local minimum in the parameter space and is unable to find the global minimum. `FullGrid` is a more computationally intensive algorithm, in which it computes the kinematic χ^2 of every model in the allowed parameter space, and gives the best fitting model. The benefit of this method is that it is much less susceptible to be stuck in a local minimum, and will usually approach the global minimum within the allowed parameter space, at the cost of much longer computation times.

In addition, models are run on only the large-scale data first, to help constrain the large-scale parameters (p, q, u, f and M/L). The inclusion of the high-resolution SIN-

FONI data does not greatly affect these parameters, particularly the dark matter parameters since we expect dark matter to be sparse in the galactic center and more concentrated at larger radii. SINFONI data is later incorporated separately, which allows us to constrain the other parameters, especially the black hole mass.

In order to incorporate the improved precision of SINFONI data at the center and to ensure we are not biased by the relatively lower quality large-scale data, we mask the large-scale data set in a central circular area of 1". This means that only the dataset that can resolve r_{SoI} is used in the very center. The masking is done by increasing the kinematic uncertainties of the large-scale dataset to 100000 within the central circle. DYNAMITE incorporates the uncertainties in each kinematic moment when calculating the kinematic χ^2, so setting a very high relative error value for certain bins means that DYNAMITE will effectively ignore it. Thus, in the combined fitting, we have a central (nearly) circular region where DYNAMITE only fits to SINFONI data, a small region where data from both SINFONI and ATLAS-3D/MUSE are equally weighted, and the outer region (for which SINFONI data does not exist, owing to its smaller angular FOV) where only the large-scale data is used for fitting.

It is also worth noting that the time taken for DYNAMITE runs can be very high. This will depend on the dataset used, the orbit library, the free parameters chosen and the mode of parameter space search chosen, but even the simplest possible run will take multiple hours to run. This is first and foremost due to the large orbit library we calculate. In a typical DYNAMITE run, we specify the different number of values each integral of motion can take. DYNAMITE will randomly sample the specified number of integrals of motion based on the allowed values. In addition, an additional parameter called `dithering` is used to check the robustness of orbits, where each orbit is shifted slightly in each coordinate direction by a number equal to the specified `dithering` value.

For example, a normal DYNAMITE run will have `nE = 21`, `nI2 = 10`, `nI3 = 7` and `dithering = 5`. Furthermore, this is done again, equally sampling from each of the three orbit families (box orbits, short axis tube orbits, long axis tube orbits) This amounts to $21 \times 10 \times 7 \times 5^3 \times 3 = 551,250$ orbits! A simple `LegacyGridSearch` run with only 3 free parameters can taken between 4 to 8 hours to complete. This will naturally increase with increase in the number of free parameters and the allowed parameter space. A `LegacyGridSearch` run with 5 free parameters can take from 7 to 15 hours to run. A `FullGrid` run is only recommended to be done on up to 3 parameters, because of the time it takes. Typically, it can take between 3 to 8 days to run. A good model is only obtained after 10-12 repeated runs of DYNAMITE, often alternating between different parameters and parameter space search modes. Thus, it can take multiple weeks to get good dynamical models of a galaxy.

Chapter 3

Results and Discussion

3.1 Results from Dynamical Modelling

Dynamical modelling was successfully completed for three of the six galaxies due to the time constraints of the thesis. As discussed in 2.5.2, DYNAMITE was run sequentially, keeping different parameters free to reduce computational time. The general strategy is first running models on only the large-scale (MUSE or ATLAS-3D) data to constrain large-scale parameters. We start with running models using the `FullGrid` mode of parameter space search on p, q and u to get constraints on the intrinsic galaxy shape. Once these are found, we try constraining M/L and f using repeated iterations of `LegacyGridSearch`. This alternating procedure is done to get a balance between reducing the time taken to compute models (using the faster `LegacyGridSearch`) and not getting stuck in various local minima (using `FullGrid`). Once the large-scale parameters are satisfactorily constrained, we add the SINFONI data and repeat the process, this time adding M_{BH} as a fitting variable. By starting with just the large-scale data, we reduce the computation time of fitting the other variables, which are not expected to change much from the inclusion of the SINFONI data (like the shape and dark matter parameters).

The best-fit values for each of the galaxies are given in Table 3.1, Table 3.2 and Table 3.3. (the errors quoted are 3σ uncertainties):

The kinematic maps for NGC 584 can be seen in Figure 3.1, Figure 3.2 (with the

Parameter name	Best fit value
f (M_{200}/M_*)	316.277
p	0.94 ± 0.05
q	0.5899 ± 0.1
u	0.98 ± 0.05
M_{BH} ($M_\odot$)	$(1.0 \pm 0.375) \times 10^8$
M/L	5.0 ± 0.4

Table 3.1: NGC 584- Best fitting Values.
χ^2/D.O.F = 1.75

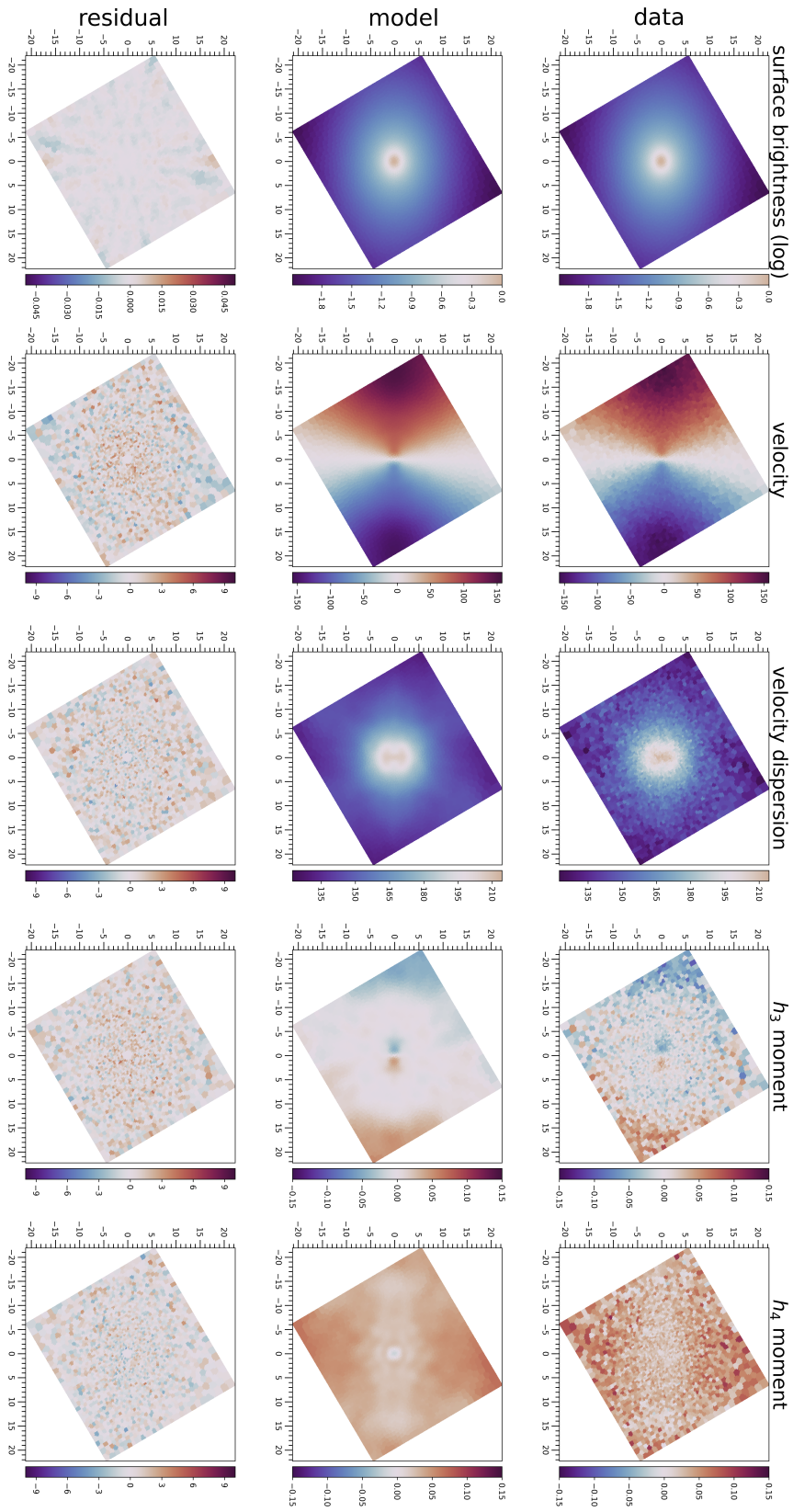

Figure 3.1: This figure shows the kinematic map for the MUSE data for NGC 584. The first row (labelled data) shows the kinematics extracted by pPXF. The second row (labelled model) shows the best-fit models found by DYNAMITE. The last row shows the data - model. Visually, it is clear that DYNAMITE has fitted the data well.

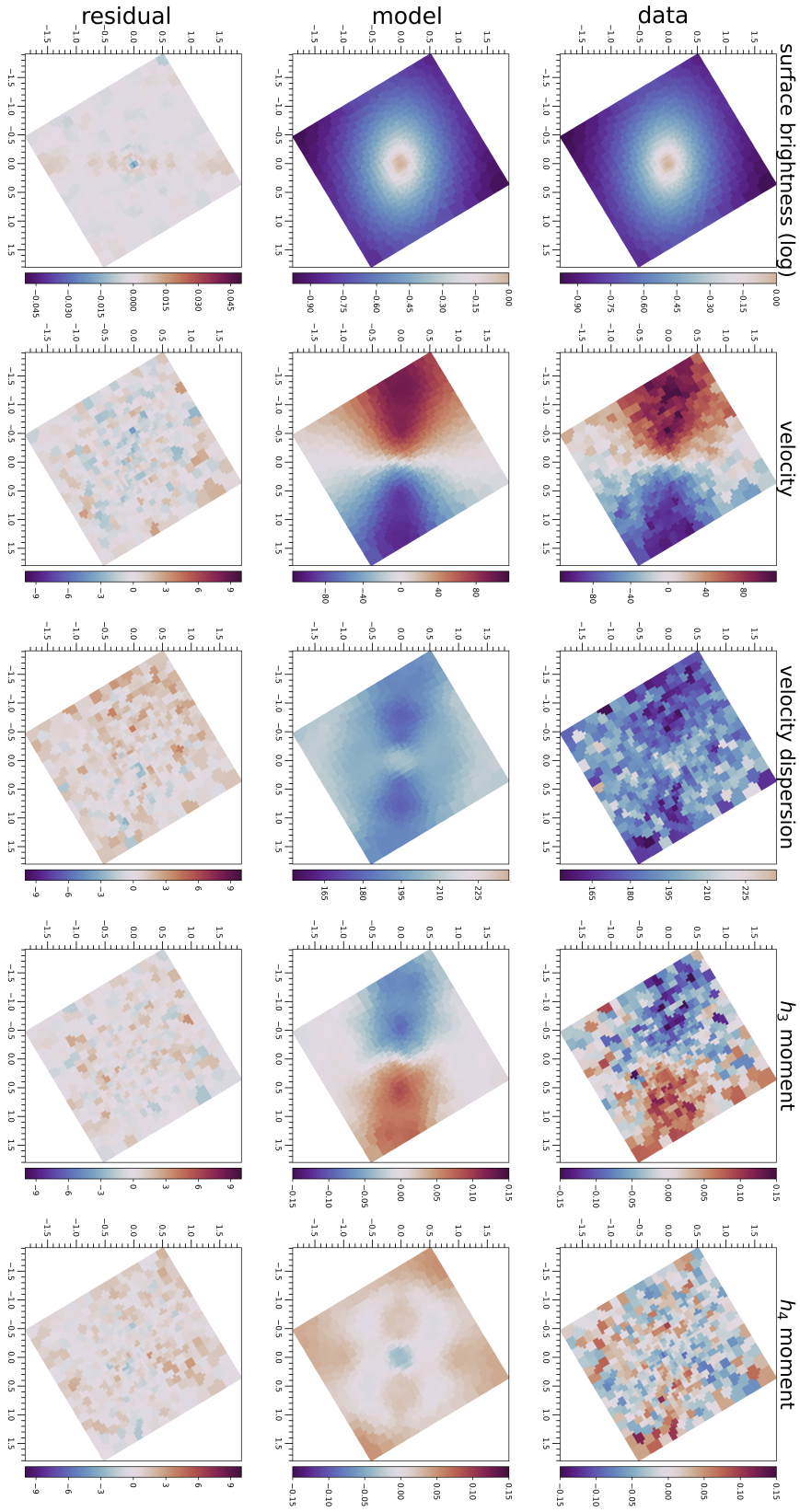

Figure 3.2: This figure shows the kinematic maps for the SINFONI data for NGC 584.

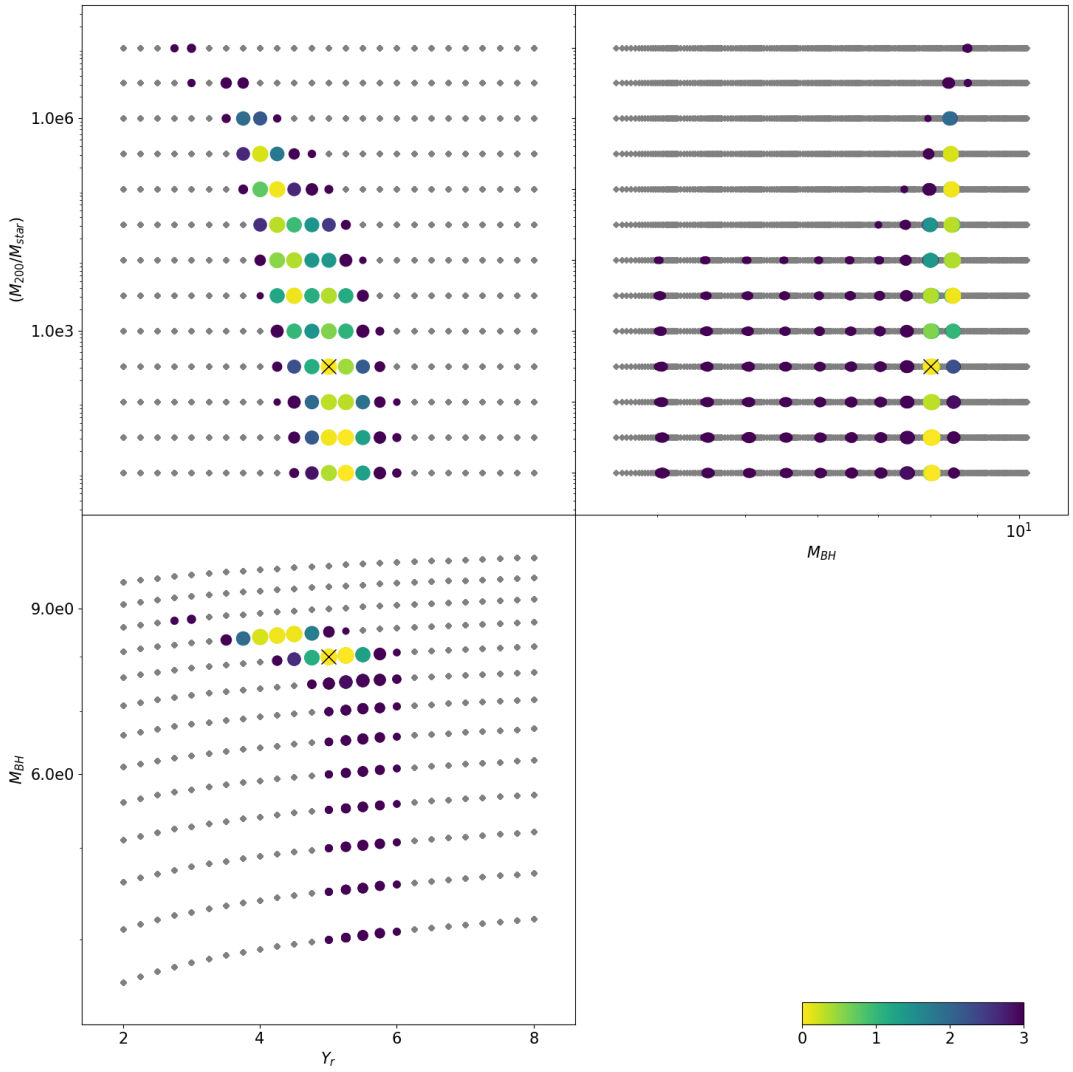

Figure 3.3: This figure shows the parameter space plot with f (denoted here as M_{200}/M_{stars}), $log(M_{BH})$ (denoted by just M_{BH} but are logarithmic values) and M/L (denoted as Y_r) for NGC 584. As we can see, the model struggles to constrain the dark matter with the characteristic large uncertainties present in the f-M/L plot.

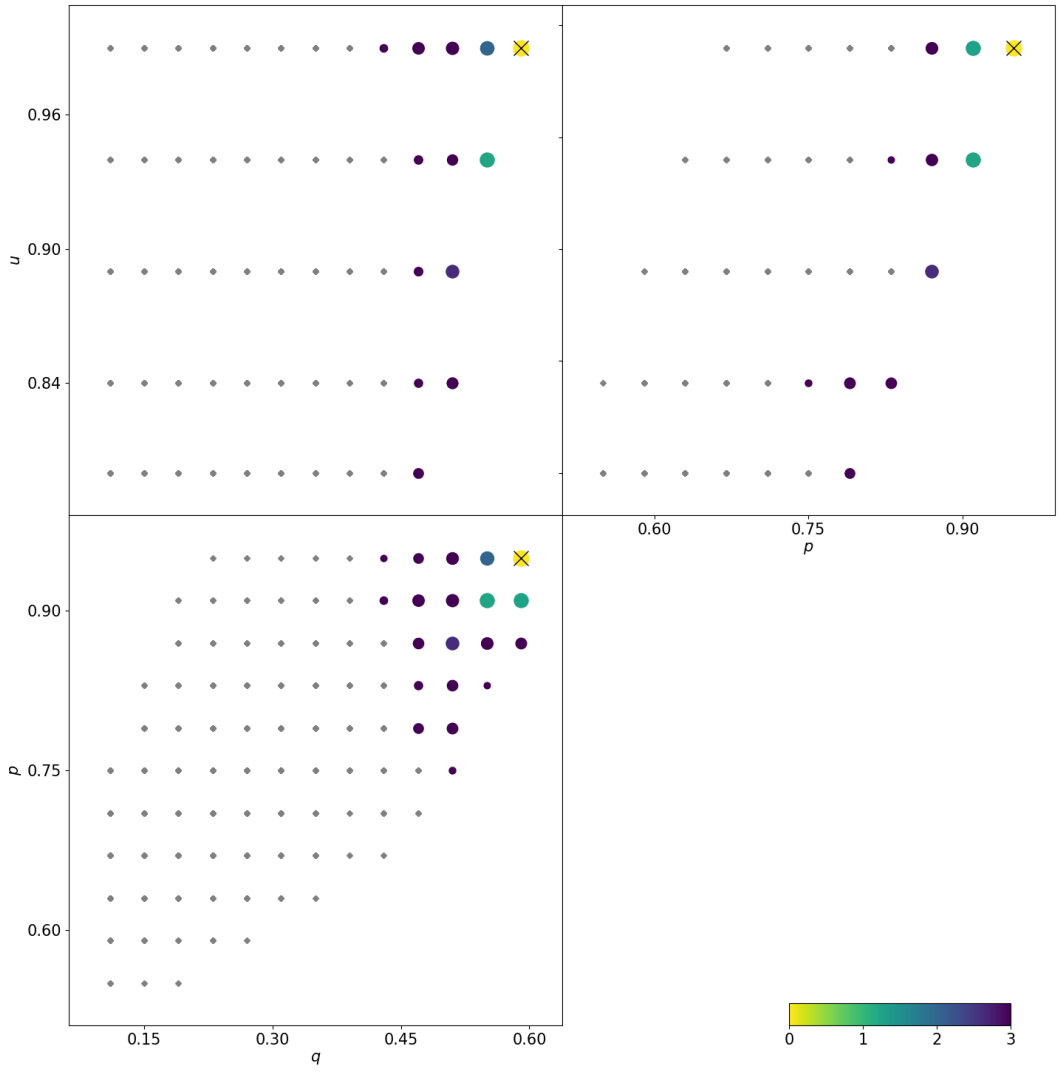

Figure 3.4: This figure shows the FullGrid parameter space plot for the triaxial shape parameters p,q and u for NGC 584.

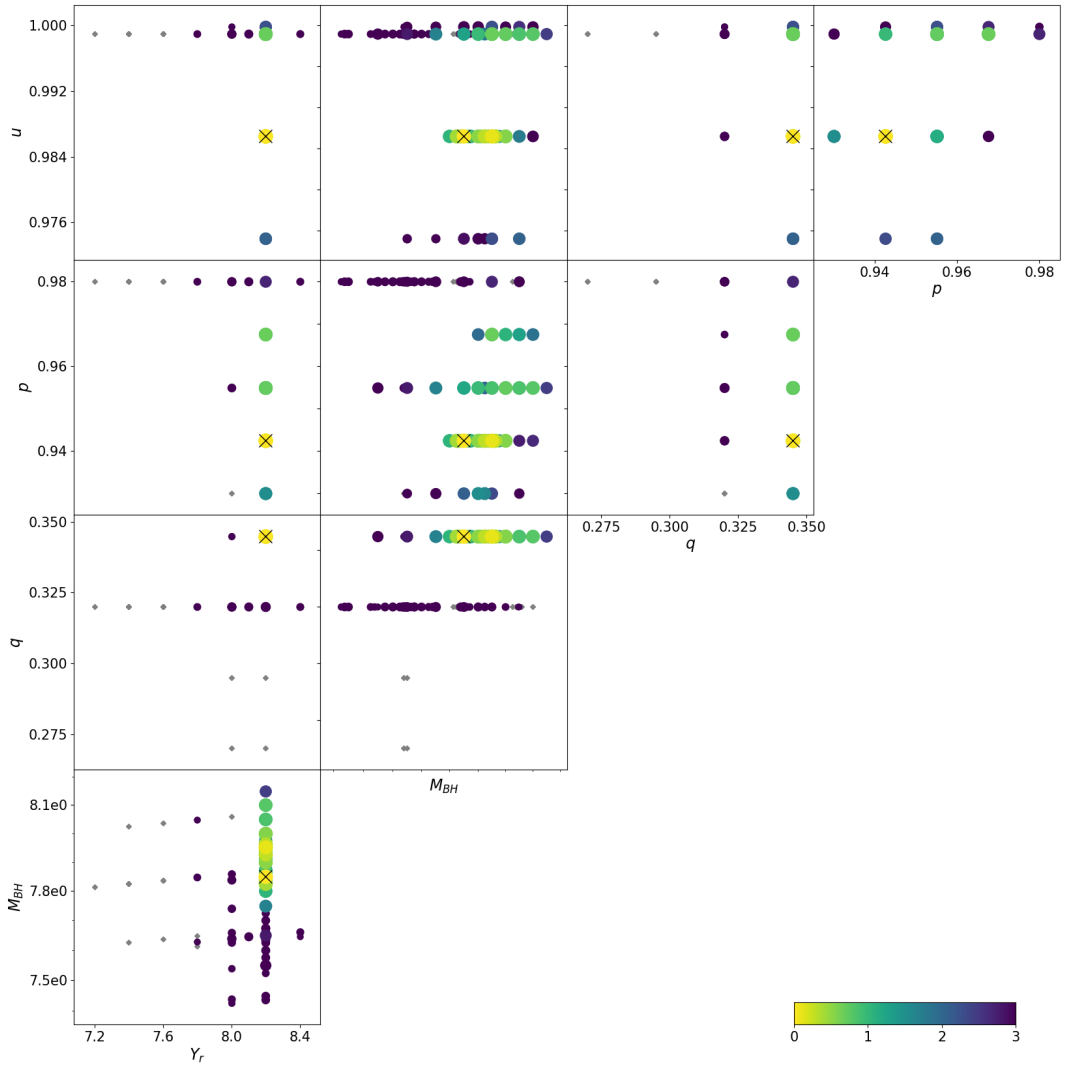

Figure 3.5: This figure shows a 5-parameter plot for NGC 4570, where p,q,u, M/L and M_{BH} were kept free. Although time-consuming, this is important to ensure that our individual best-fit parameter values are also a global minimum in the full parameter space.

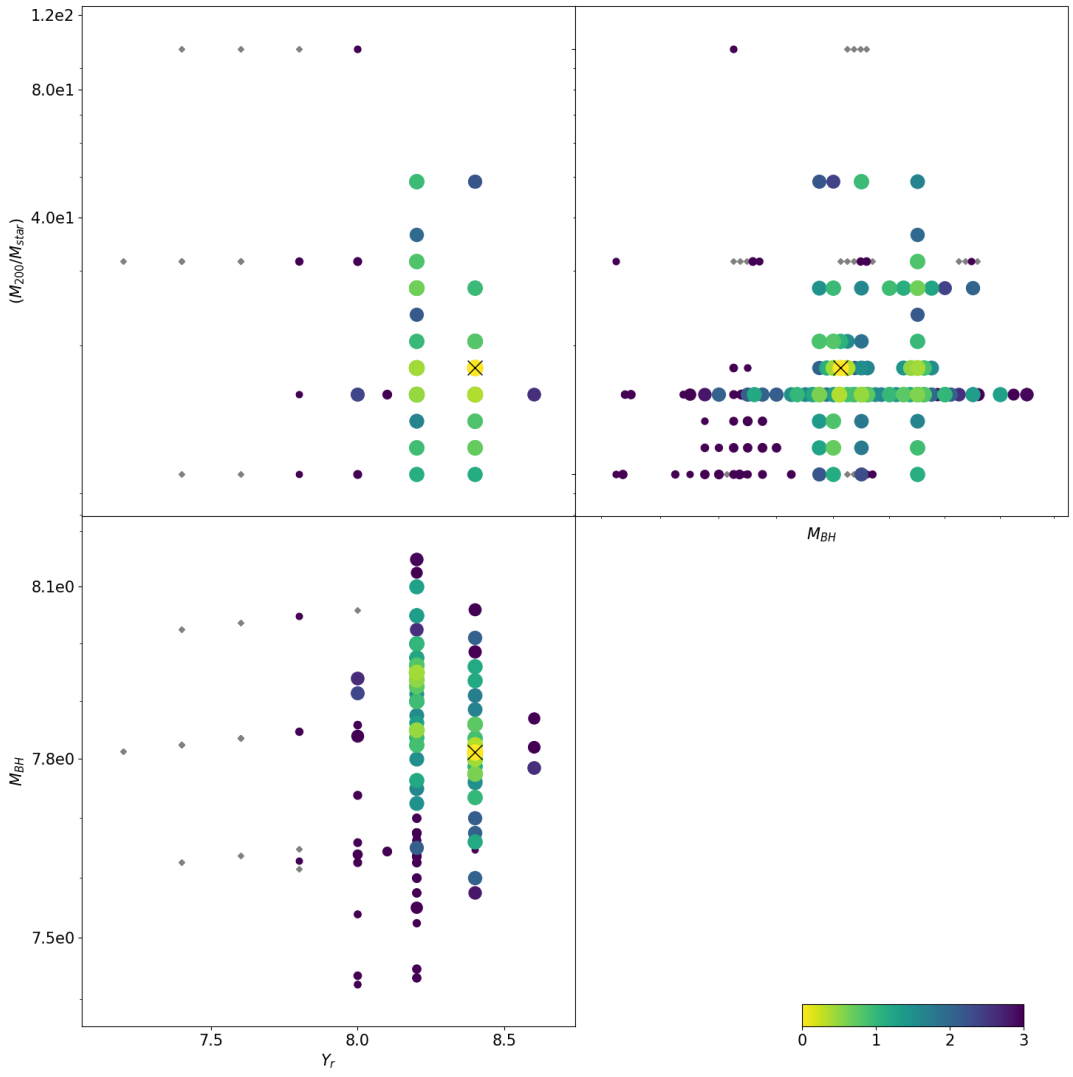

Figure 3.6: This figure shows the best-fit values for f,M/L and M_{BH} for NGC 4570.

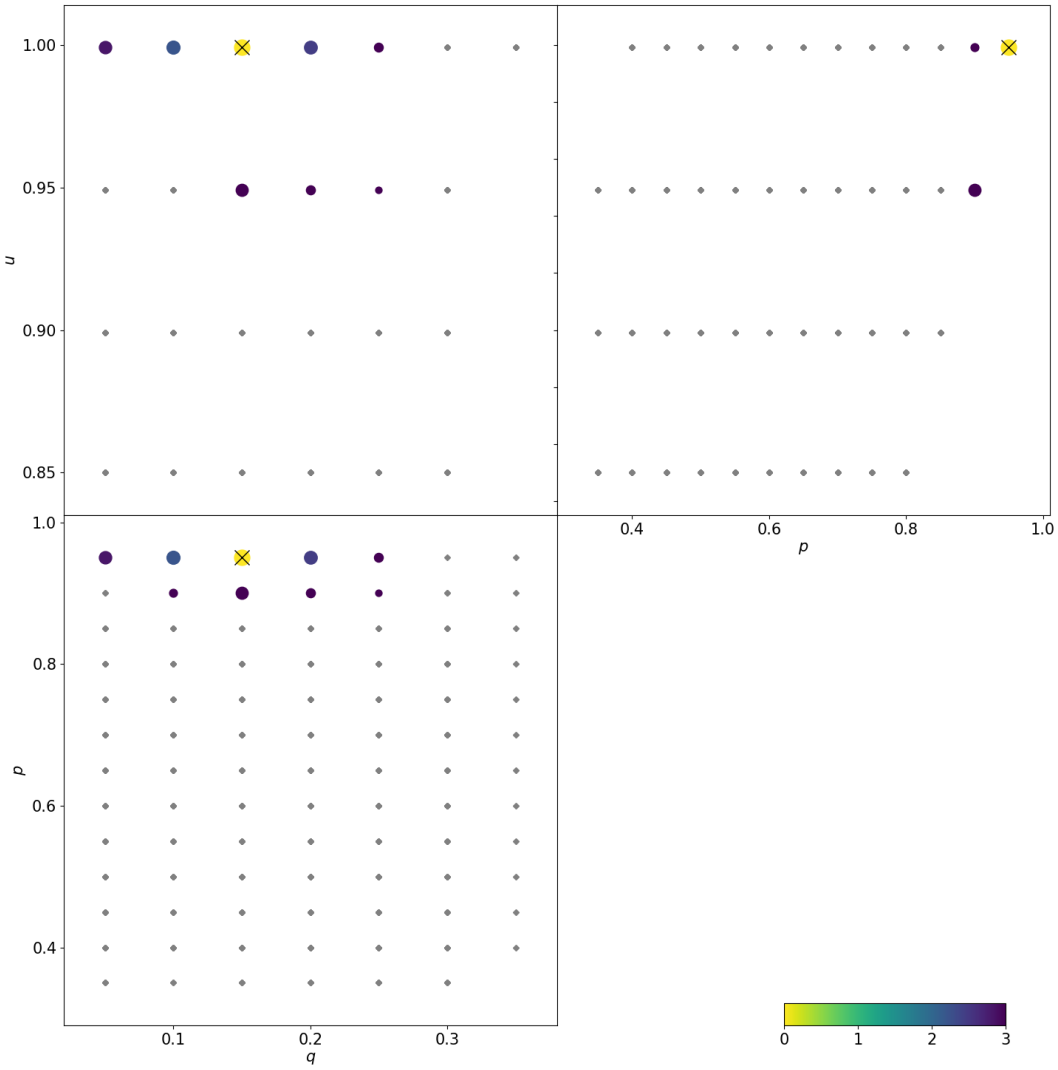

Figure 3.7: This figure shows the best-fit values for p,q and u (the shape parameters) for NGC 4281.

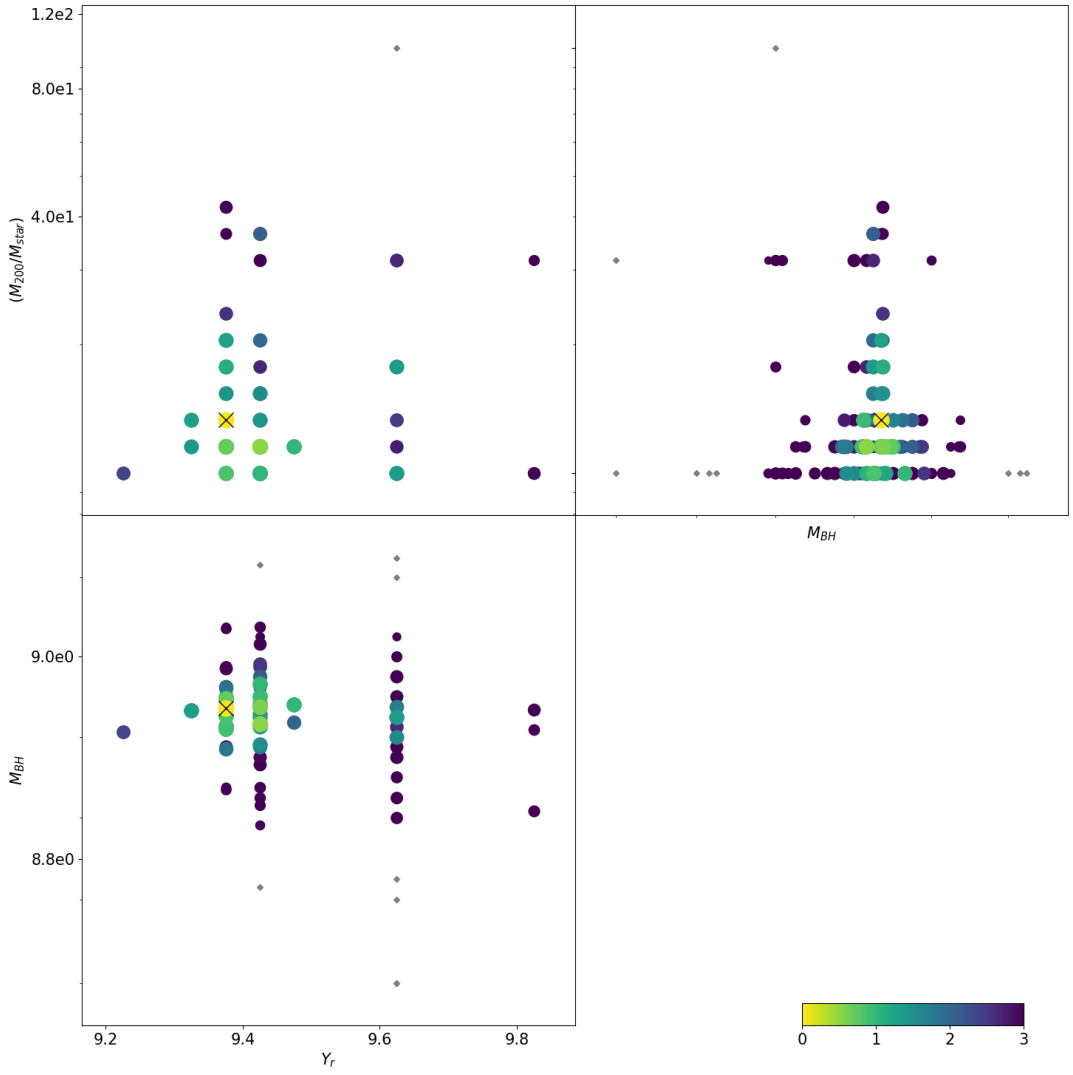

Figure 3.8: This figure shows the parameter space plot for M_{BH}, M/L and f for NGC 4281.

Parameter name	Best fit value
f (M_{200}/M_*)	17.78
p	0.9425 ± 0.05
q	0.345 ± 0.1
u	0.9865 ± 0.05
M_{BH} $(M_\odot)$	$(6.49 \pm 0.4) \times 10^7$
M/L	8.4 ± 0.3

Table 3.2: NGC 4570- Best fitting Values.
χ^2/D.O.F = 1.80

Parameter name	Best fit value
f	13.33
p	0.95 ± 0.05
q	0.15 ± 0.05
u	0.99 ± 0.05
M_{BH} $(M_\odot)$	$(8.66 \pm 0.4) \times 10^8 M_\odot$
M/L	9.375 ± 0.2

Table 3.3: NGC 4281- Best fitting Values.
χ^2/D.O.F = 1.21

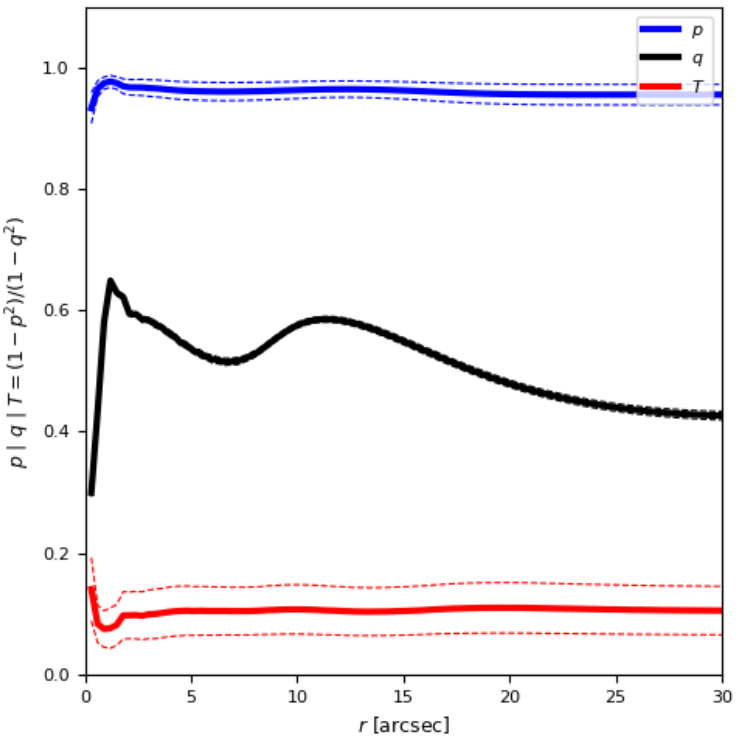

Figure 3.9: This figure shows the radial profile of the shape parameters for NGC4570. T is the triaxiality parameter, where the galaxy is perfectly axisymmetric at T=0, and approaches 1 as it becomes more and more triaxial. The sharp jump around 1 arcsec is due to the plot jumping from SINFONI to ATLAS-3D data.

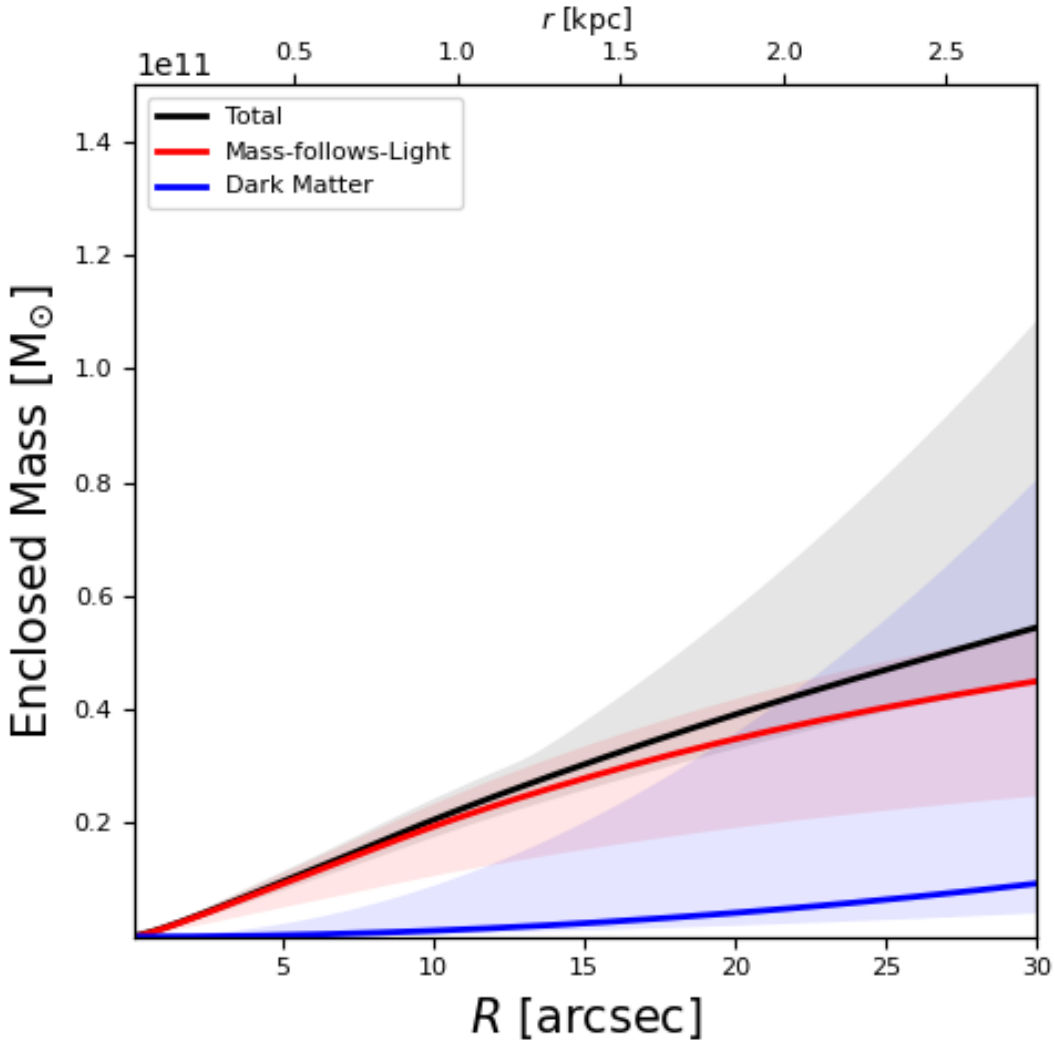

Figure 3.10: This figure shows the radial profile of total mass. luminous mass (mass-follows-light) and dark matter mass for NGC 584. As we can see, the total mass has a significant effect from dark matter at large radii. The uncertainties increase towards larger radii because of the reduction in the amount of tracers as we go to larger radii.

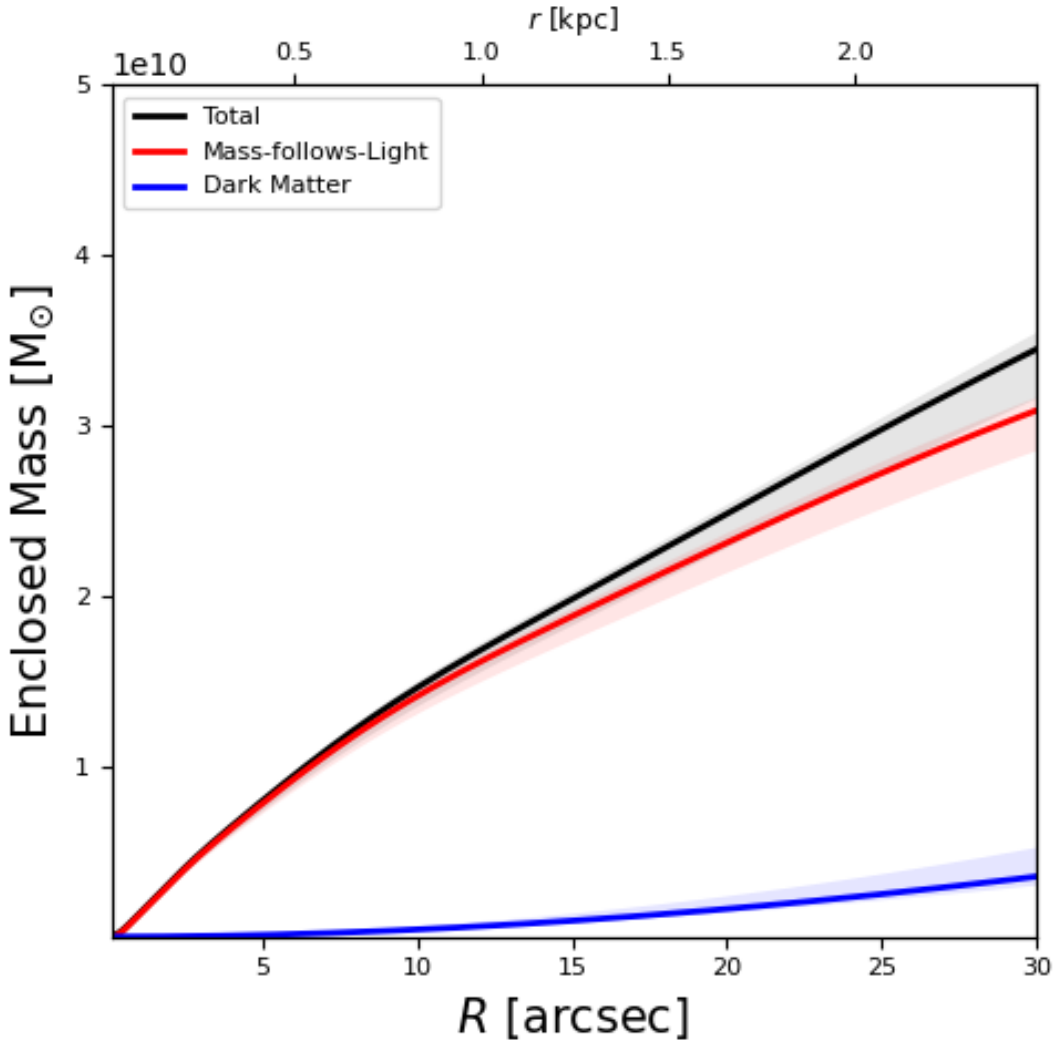

Figure 3.11: This figure shows the radial profile of total mass, luminous mass (denoted by mass-follows-light), and dark matter mass for NGC 4570. In comparison to NGC 584, we can see that the dark matter fraction is much lower, and has a lower effect on the total mass.

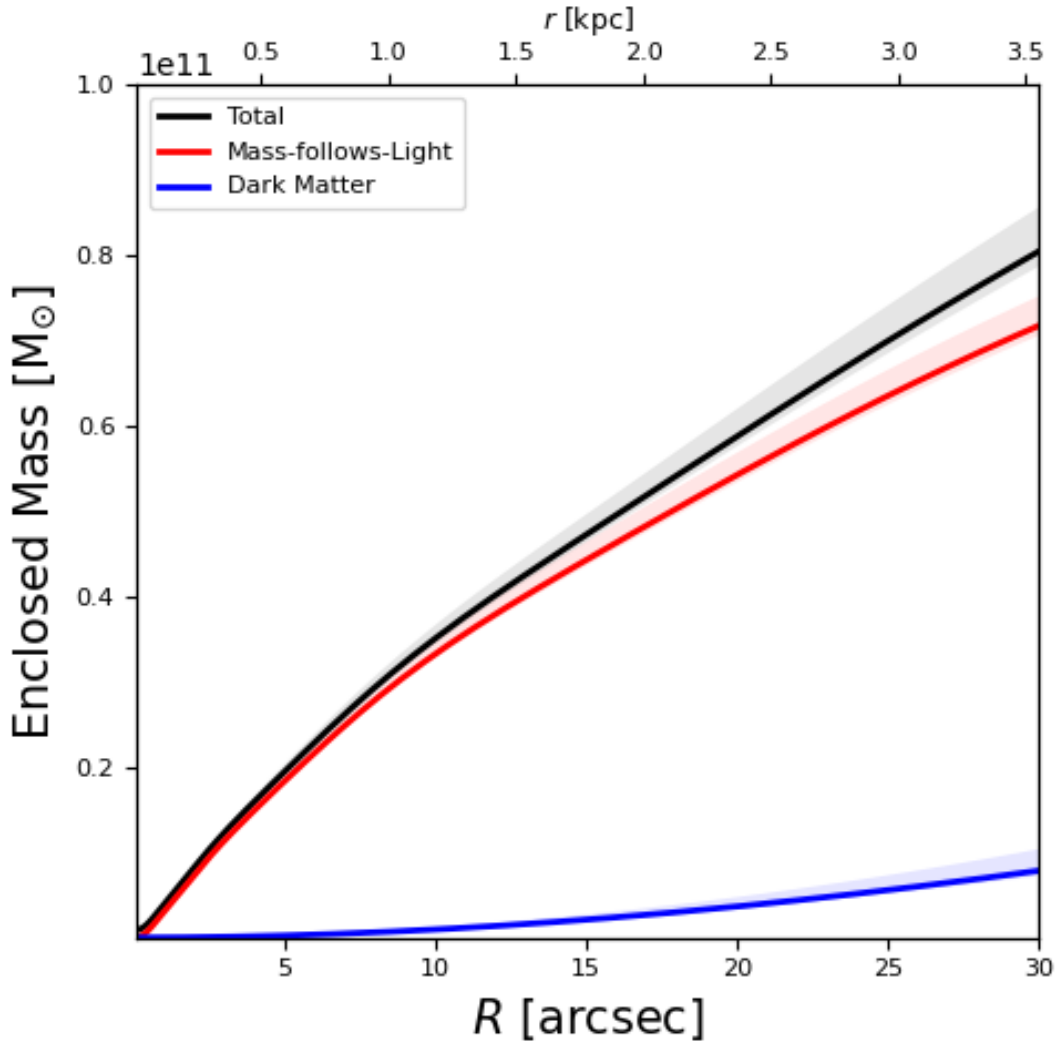

Figure 3.12: This figure shows the radial profile of total mass, luminous mass (denoted by mass-follows-light) and the dark matter mass for NGC 4281.

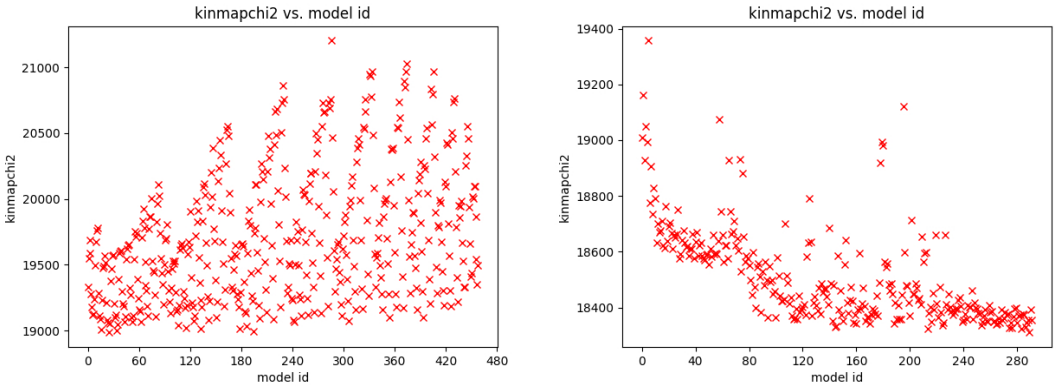

Figure 3.13: This figure shows the plot of kinematic χ^2 versus time (model_id signifies the sequence at which they are generated) for NGC 4570. The left plot is for the FullGrid mode of parameter space search. Since FullGrid does not actively search for the best model, it appears to be random. The right plot is for the LegacyGridSearch mode, which has an algorithm to converge to the best-fit or lower kinematic χ^2, which can be seen in the plot.

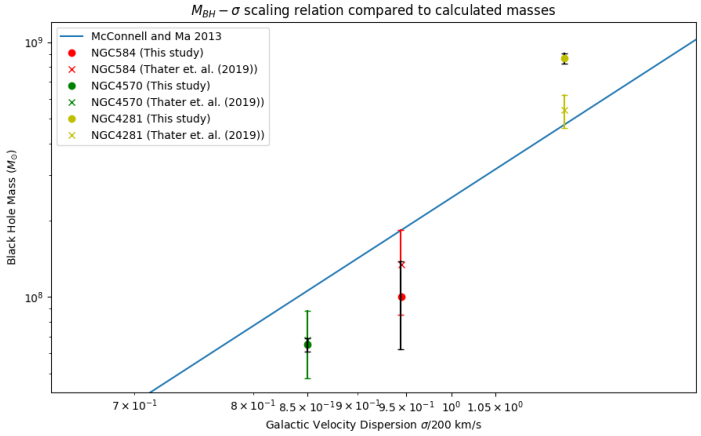

Figure 3.14: This plot shows the measured SMBH masses (represented by dots) compared to a measured scaling relation [50] (represented by the line) and the SMBH mass measurements from [1] (represented by crosses). All values are close to the scaling relation and are consistent with it.

kinematic maps for the other galaxies in Appendix A). These maps help us get a visual understanding of how well our best-fit models reproduce the flux map as well as the kinematic moments. On the other hand, it can also help us identify some unique physical features in our galaxy, such as hints towards possible substructures or other sources of error (such as foreground objects that may interfere with the fitting) that are otherwise difficult to identify. The parameter space plots give a more quantitative look at what DYNAMITE does and help us gain insight into if we have a good model and if it could be improved. For example, as shown in the plots, if the best-fit model is not surrounded by a smooth gradient of similarly well-fitted models (slightly higher kinematic χ^2), it is possible it is a local minimum, not a global minimum. These plots also give us insight into what parameters are difficult to constrain and would have high uncertainties. For example, dark matter parameters are difficult to constrain, and this can be seen with the large number of models that are quite far from the best-fit model in the parameter space but have almost the same kinematic χ^2. Furthermore, it also tells us about which parameter, when changed, can cause large changes in the best-fit values of other parameters. This is usually M/L, which can, in turn, change f as well as the shape parameters.

We expect to see some general trends in each type of output plot that serve as a way to confirm if our models are working as expected. The most common one is the anti-correlation between V and $h3$ in the kinematic maps, signifying that the mean velocity has a skew in that direction. Another general trend we see (especially when using tracers that cannot map the dark matter halo well, like stars) is the degeneracy between the black hole mass, M/L and dark matter mass. The dynamical modelling algorithm cannot differentiate well if the mass it 'sees' should be accounted for by the stars, the black hole or the dark matter.

The parameter space plots (for example, Figure 3.7) are not trivial to interpret and need some explanation. If a run of DYNAMITE contains n free parameters, a parameter space plot of $\binom{n}{2}$ subplots is created. Each plot has the same number of dots, with each dot representing multiple models run by DYNAMITE. The color of the dot represents how good the model is. A yellow dot with a cross on it is the best-fit model, or the model with the lowest kinematic χ^2. The other colors represent how far in kinematic χ^2 from the best-fit model a given model is, with the colorbar showing the statistical significance. Smaller grey dots represent models that are further than 3σ confidence interval from the best-fit model, and these can generally be considered as bad-fitting models.

Figure 3.9 shows the changing triaxiality with radius. In general, the triaxiality parameter is not constant throughout the galaxy and is expected to change slightly with radius. NGC 4570 shows a particularly sharp jump (especially in q) around 1", which may be the cause of the M/L discrepancy (discussed in 3.2.2).

Figure 3.10, Figure 3.11 and Figure 3.12 show the cumulative (or enclosed) mass profiles with radius. As Dark Matter is modelled as a NFW halo, we can see that it only

becomes influential at very large radii. As NGC 584 has a much higher best-fit dark matter fraction value, we can see that the dark mass starts to dominate the total mass much more quickly. The comparatively lower uncertainties in NGC 4570's enclosed mass profile are most likely due to the fewer number of models run for that galaxy, causing DYNAMITE to underestimate the size of the error bars.

Figure 3.13 shows us how the modelling algorithm proceeds in both types of parameter space search modes. These plots help us get an understanding of how many models have been run, while also telling us about the time taken to compute these many models. In general, a higher number of models would have taken a larger amount of time to calculate, and for `FullGrid` runs with ≈ 400 models or more, it often takes more than 4 days to calculate all of them. Looking at the Progress plot for `LegacyGridSearch` models can also give a hint towards whether we have reached our best possible model. If the progress plot has saturated and does not show any signs of reduction despite multiple runs, it is a hint that the algorithm has found a global (or local) minimum. In the case of 3.13, we can see that the models have started to saturate but may still reduce slightly more, indicating that more models need to be run before a proper conclusion can be made.

Figure 3.14 shows how the measured SMBH masses in this study as well as the previous measurements from [1] compare to the known M_{BH} - σ scaling relation [50]. As is clear from the plot, my measurements are mostly consistent with the previous study as well as the known scaling relation.

3.2 Discussion

3.2.1 NGC 584

NGC 584 was the first galaxy analyzed in this work. As such, significantly more time was spent on redoing pPXF fitting and doing test DYNAMITE runs to get a better understanding of the processes and techniques involved. It was also the galaxy that had the most models (≈ 1000) run for it. Owing to the fact that this galaxy was the only one whose large-scale data came from MUSE, it has much better spatial resolution (in the large-scale data) compared to the other galaxies (0.2×0.2 arcsec pixel size for MUSE compared to 0.94×0.94 arcsec for ATLAS-3D).

The first conclusion that can be made about this galaxy is that dynamical modelling gives further evidence that this galaxy is (almost) axisymmetric. Since $p = 0.95$, which is very close to 1, that means that the two longer axes (b and a) are almost equal in length, implying axisymmetry. This means that performing a comparison with [1] is valid since that study assumed all the galaxies were axisymmetric. The best-fit value for dark matter fraction is much higher than the other galaxies studied. However, due to the inability of DYNAMITE to constrain dark matter parameters given the smaller available FOV and lack of other tracers like Globular Clusters, it is entirely possible for the real value to be much more sensible.

Compared to [1], this galaxy is relatively consistent with the values presented in that study. M/L is slightly lower at 5.0 $M_\odot/L_\odot$ from 5.4 $M_\odot/L_\odot$ in [1]. This is an expected effect, because the model assigns more of the mass to dark matter in the current study, whereas [1] assumes all the mass is baryonic and must require a higher M/L to recreate the observed kinematics. The black hole mass is also very close ($1 \times 10^8 M_\odot$ compared to $1.34 \times 10^8 M_\odot$). While more models would be needed to determine exactly how significant this deviation is, it is likely consistent within the bounds of our measurement error. In this case, the effect of the inclusion of dark matter is not too significant, and while including the added degree of freedom from triaxiality gives evidence of the galaxy's intrinsic shape being actually close to axisymmetric, does not deviate from the previously measured from the SMBH mass.

As seen in the kinematic maps in Figure 3.1 and Figure 3.2, there is a conical shape present in the centre of the velocity dispersion map. This particular feature points to the presence of a disk in the galaxy, giving further evidence to the fact that NGC 584 is a lenticular (S0) galaxy and not a pure elliptical.

3.2.2 NGC 4570

NGC 4570 was the second galaxy studied in this work. Since the large-scale data for this galaxy was taken from ATLAS-3D/SAURON, it has worse spatial resolution and generally higher noise than the MUSE data. However, since the number of bins is significantly lower, it often leads to much lower overall χ^2 values. Along with NGC 4281, this galaxy has a very low value of best-fit dark matter (f), but this can again be due to the poor constraint on dark matter imposed by our dynamical modelling, particularly since we use stellar kinematics within 1 effective Radius.

This galaxy shows the most deviation from the values presented in [1]. The SMBH mass is mostly the same (within error bounds) ($6.7 \times 10^7 M_\odot$ from this work compared to $6.8 \times 10^7 M_\odot$ in [1]). The deviation is interestingly in M/L (8.4 $M_\odot/L_\odot$ is the best-fit value compared to 5.5 $M_\odot/L_\odot$ from [1]). It is much *higher* when we would expect a slightly lower M/L after the inclusion of dark matter. The dark matter content is also quite low and one wouldn't expect a significant M/L drop from the dark matter that the best-fit model predicts, but such an increase in M/L is not expected and warrants further investigation. If this is not caused by a systematic error, it can be caused due to M/L gradients present in the galaxy. Interestingly, the models run on just the large-scale ATLAS-3D data, the M/L settled to a much more consistent value of 5.25 $M_\odot/L_\odot$. The inclusion of the high-resolution SINFONI data somehow changes the best-fit value of M/L greatly. Further study of this galaxy is required before any concrete conclusions can be made.

3.2.3 NGC 4281

NGC 4281 was the third galaxy studied in this work. The large-scale data taken from ATLAS-3D/SAURON has a worse resolution than NGC 584, but it has relatively bet-

ter quality data (and less noise) compared to NGC 4570. However, it also contains a prominent foreground object (most likely a Milky Way star) in the ATLAS-3D data that needed to be masked in a similar procedure to masking the central region when incorporating SINFONI data.

NGC 4281 has the highest deviation in terms of SMBH mass of the three galaxies in this work from [1] ($8.66 \times 10^8 M_\odot$ in this work as compared to $5.43 \times 10^8 M_\odot$ in [1]). The M/L is almost exactly the same, as expected from the very low dark matter content in the best-fit model. It is unclear what the reason for the discrepancy in the SMBH mass measurement could be. The most plausible reason could be the fact that [1] used symmetrized kinematics as the kinematic data (in other words, the values of each kinematic moment above and below the rotational major axis are averaged to give a more homogenous kinematic map). This process can sometimes cause large deviations in the observed parameters. Another reason could be the fact that DYNAMITE is stuck in a local minimum and unable to find the global minimum which might be much closer to the established value from [1]. Further study would be required to determine the reason behind this discrepancy.

3.2.4 Sources of Error

As with any scientific method, finding SMBH masses is sensitive to a variety of error sources that will be briefly discussed in this section. While the pPXF routine, as well as Adaptive Optics, helps mitigate a number of large sources of error like the atmosphere and dust, some effect of these may still cause spurious spectral lines to occasionally seep through into our data. Voronoi binning also helps to further combat this by maintaining a minimum S/N in the kinematics. There are some sources of error that cannot be accounted for by the methods discussed above, however. The biggest one is the distance to the galaxy. DYNAMITE requires the distance to the galaxy as an input, which we take from existing literature on our galaxies (see [1] for details). An incorrect distance can have a large effect on our measured SMBH mass. The angle of inclination is also a very important source of uncertainty. Large inclination angles (i.e. a very face-on galaxy) can also lead to high uncertainties in our observed kinematics, which will lead to very poor constraints on any galaxy parameter.

3.2.5 Future Work

In order to confirm the results of this study until now, some additional research and analysis is required, which will be discussed in this section.

First, the uncertainties for the best-fit values need to be precisely calculated. This will help us quantify how significant the differences we see actually are. This requires more models to be run, whose time requirements would have been out of the scope and duration of this thesis. While we do not expect the best-fit values to change much while running more models, the preliminary error estimates may still change after more

models are run, likely because of the complex nature of the parameter space.

Second, the sample of galaxies studied is planned to be increased. This study will soon be extended to the remaining three galaxies from the sample in [1]. This will give us a better understanding of which values are consistent and which are not, and can give us hints towards any patterns that may arise from the triaxial dynamical modelling these three galaxies, and is, in fact, shown to be quite common [48, 1].

The complexity of the models can also be increased. As discussed earlier, the sudden jump in M/L in NGC 4570 is likely due to M/L gradients being present in the data. This can be better understood if we model M/L as a radially changing function instead of a constant value throughout the galaxy. Because of the difference in stellar populations with respect to radius in most galaxies, radially varying M/L can often be a more realistic model of the galaxy [51].

As mentioned previously, all three galaxies' shape parameters confirm that these particular galaxies are indeed axisymmetric, which means that axisymmetric Schwarzschild modelling is a valid approach for them. It will also be worthwhile to extend this comparison to more triaxial early-type galaxies and see if this method is able to constrain SMBH masses as accurately. Although it is not always easy to tell the 3-dimensional structure of a galaxy without some form of dynamical modelling, more triaxiality is expected in slow rotators (galaxies with comparatively very little rotational velocities). More triaxial galaxies can be used to check the generality of triaxial Schwarzschild modelling.

The effect of dark matter on SMBH mass measurements still poses some mysteries that also provide an avenue for future work. While stellar kinematics-based dynamical modelling struggles to constrain dark matter, higher quality data from future telescopes can always increase our accuracy. Including other tracers like Globular Clusters and H-I gas can also improve the constraints on dark matter. Even so, the degeneracy between M/L, M_{BH} and dark matter remains an issue at small and intermediate radii, where DYNAMITE is unsure whether the mass that contributes to the kinematics should belong to the stars, the dark matter halo or the black hole.

Chapter 4

Conclusion

In conclusion, I measured the SMBH masses of three galaxies; NGC 584, NGC 4570 and NGC 4281; using a dynamical modelling method. More specifically, a Python and FORTRAN based routine called DYNAMITE was used to perform triaxial Schwarzschild modelling to constrain these SMBH masses. The SMBH masses were calculated to be $(1.0 \pm 0.375) \times 10^8 M_\odot$ for NGC 584, $(6.49 \pm 0.4) \times 10^7 M_\odot$ for NGC 4570 and $(8.66 \pm 0.4) \times 10^8 M_\odot$ for NGC 4281. This study was a comparison study as well as a generalization of the work done in [1], which had two strong assumptions that were relaxed in this work. Firstly, it assumed that all these galaxies are axisymmetric. Secondly, it did not account for the effect of dark matter. This work models galaxy shape as triaxial, and includes a spherical NFW halo as the dark matter model.

All three galaxies were found to be axisymmetric, or very close to it ($p > 0.95$ for all three galaxies). This confirmed the assumption made in [1] as well as validated the comparison. Furthermore, two of the three SMBH masses (NGC 584 and NGC 4570) were very close and hence consistent with the measurements in [1]. The SMBH mass of NGC 4281 was slightly higher than the measurement in [1], the exact cause of which is still unknown and warrants further study. Moreover, while the SMBH mass stayed consistent, the Mass-to-Light ratio of NGC 4570 turned out to be much higher than the one reported in [1]. The cause of this is also unconfirmed, but is likely due to M/L gradients present in the data. Further investigation of this galaxy is also needed to find a cause for this.

This work can be extended by applying the methods used in this study to other galaxies, particularly the remaining galaxies from [1]. It can also be extended by considering more complex models (radially varying M/L, 2 parameter NFW halos etc.) or with higher FOV and higher spatial resolution data to get better data on kinematics. Furthermore, other tracers can also be included to allow us to further constrain other parameters like dark matter.

Appendices

Appendix A

Additional Plots

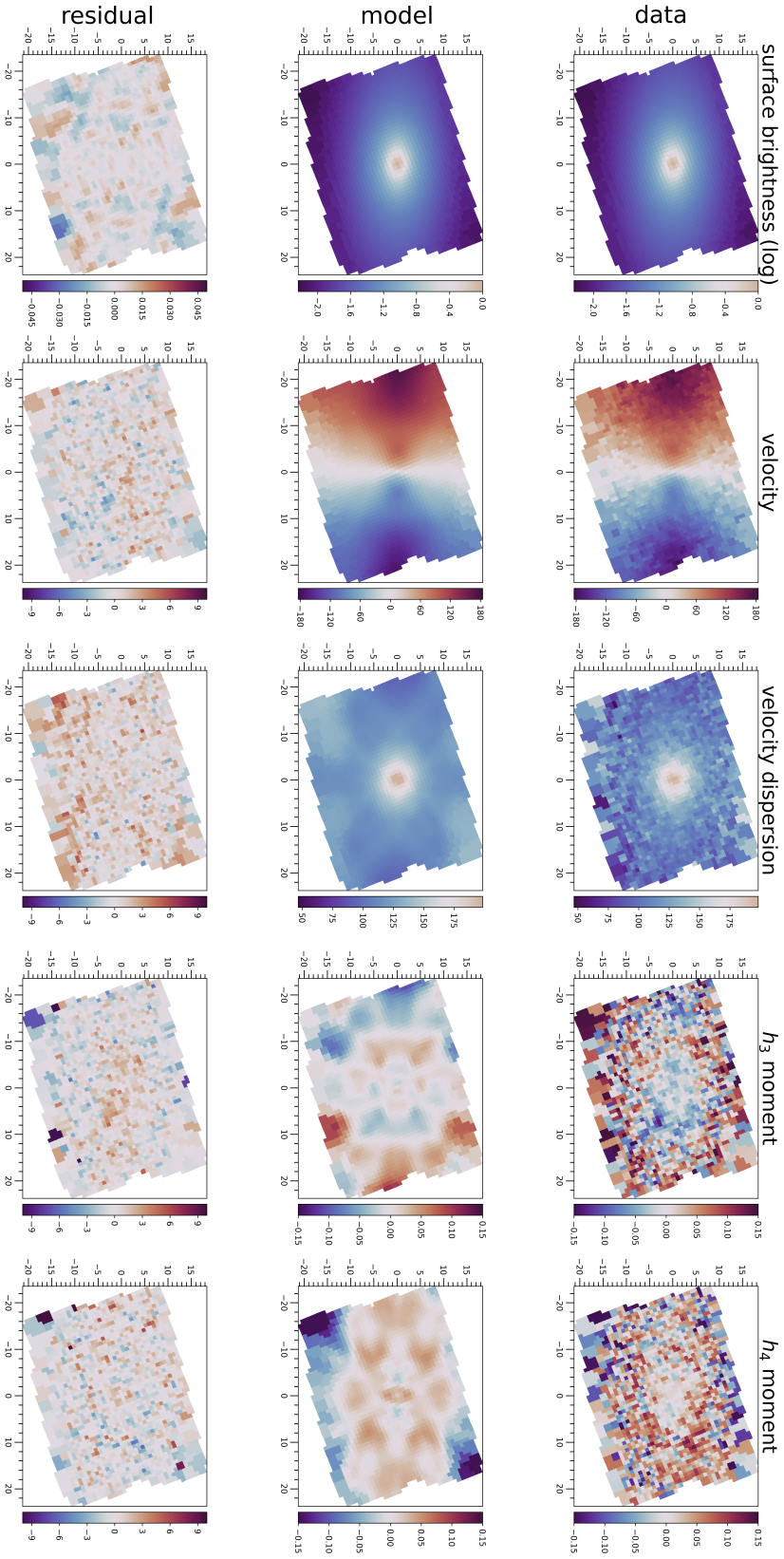

Figure A.1: This figure shows the kinematic maps for each kinematic moment for NGC 4570 from ATLAS-3D data. The lower spatial resolution and lower S/N compared to MUSE is visible here.

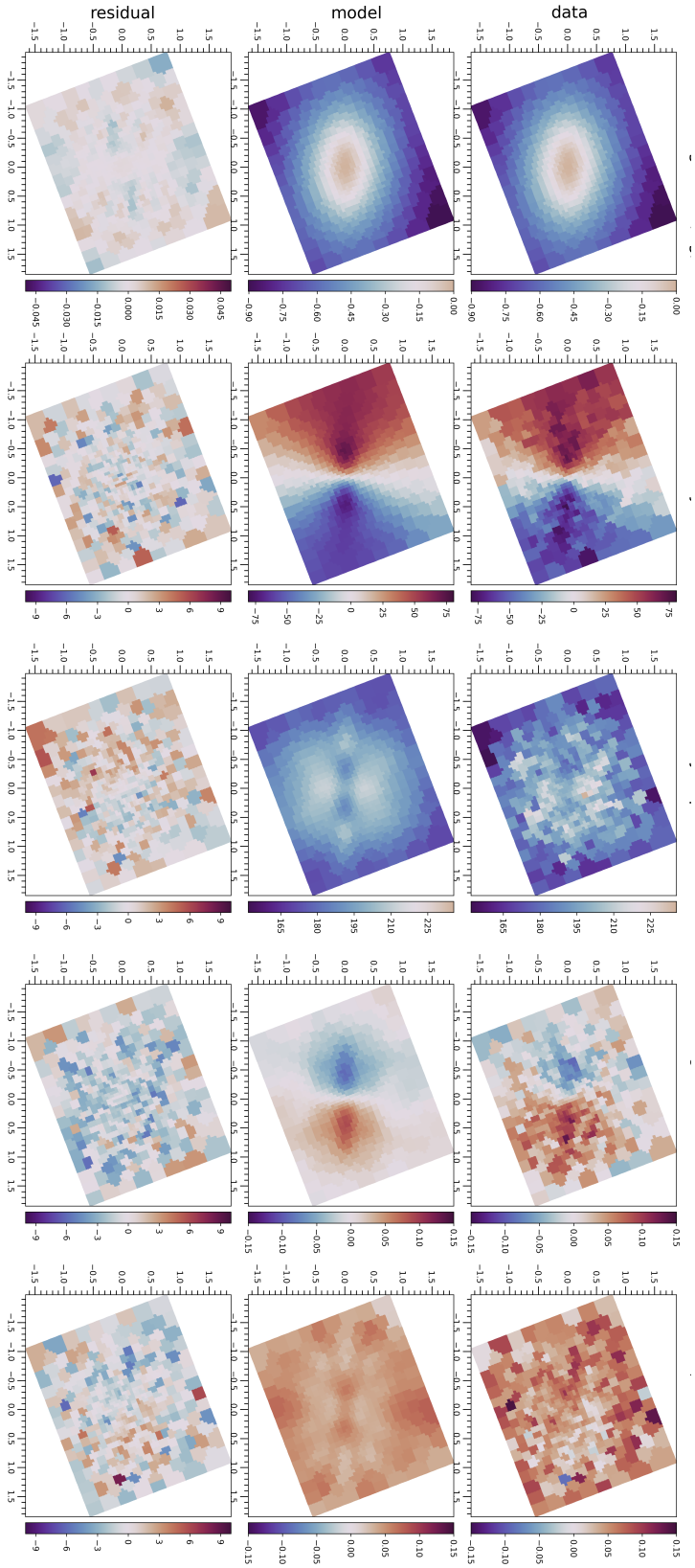

Figure A.2: This figure shows the kinematic maps for each kinematic moment for NGC 4570 from the high-resolution SINFONI data.

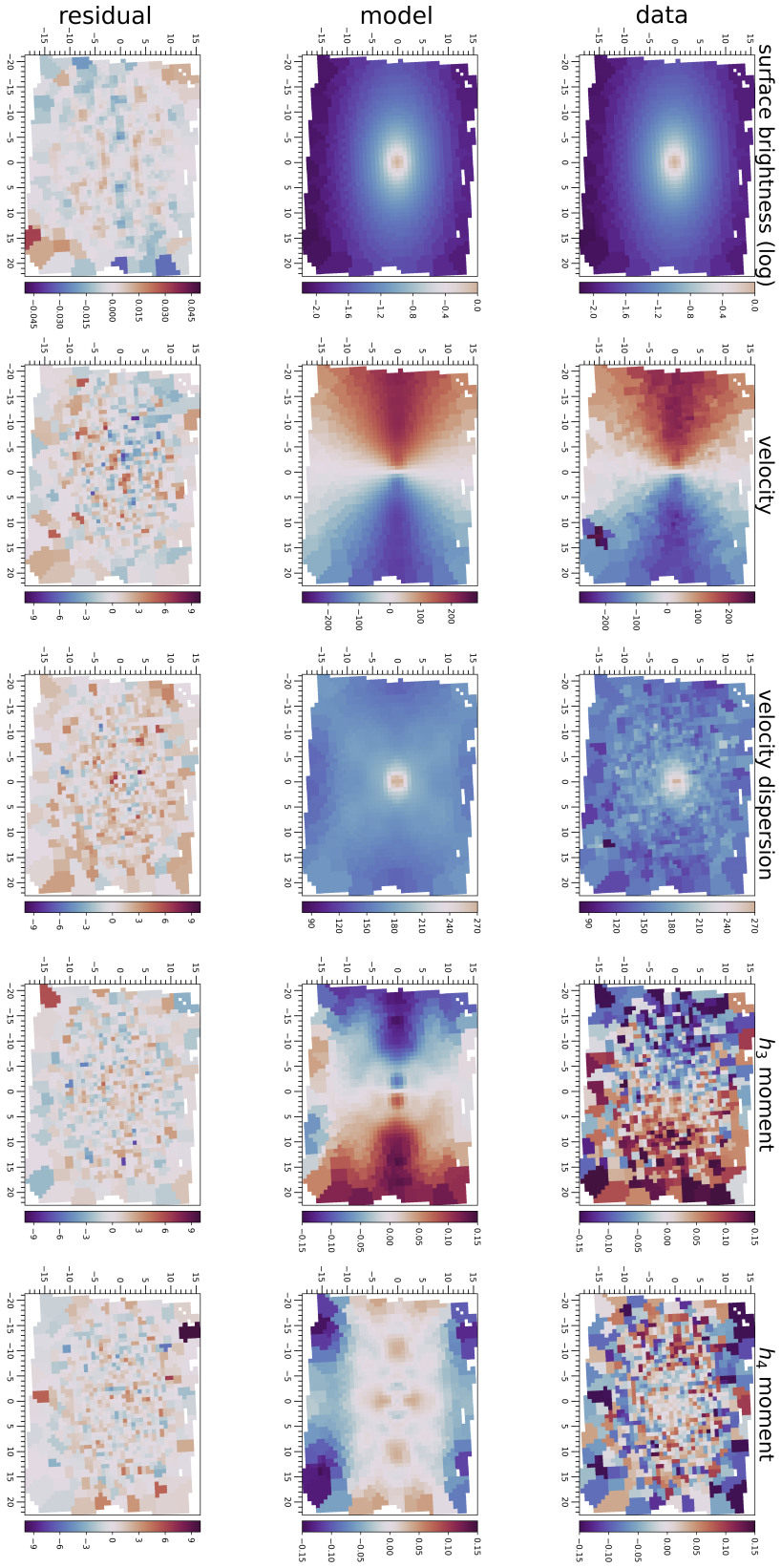

Figure A.3: This figure shows the kinematic maps for each kinematic moment for NGC 4281 from the large-scale ATLAS-3D data. The foreground object (visible in the Mean Velocity map as a spot of exceptionally negative velocity) was masked during the fitting procedure.

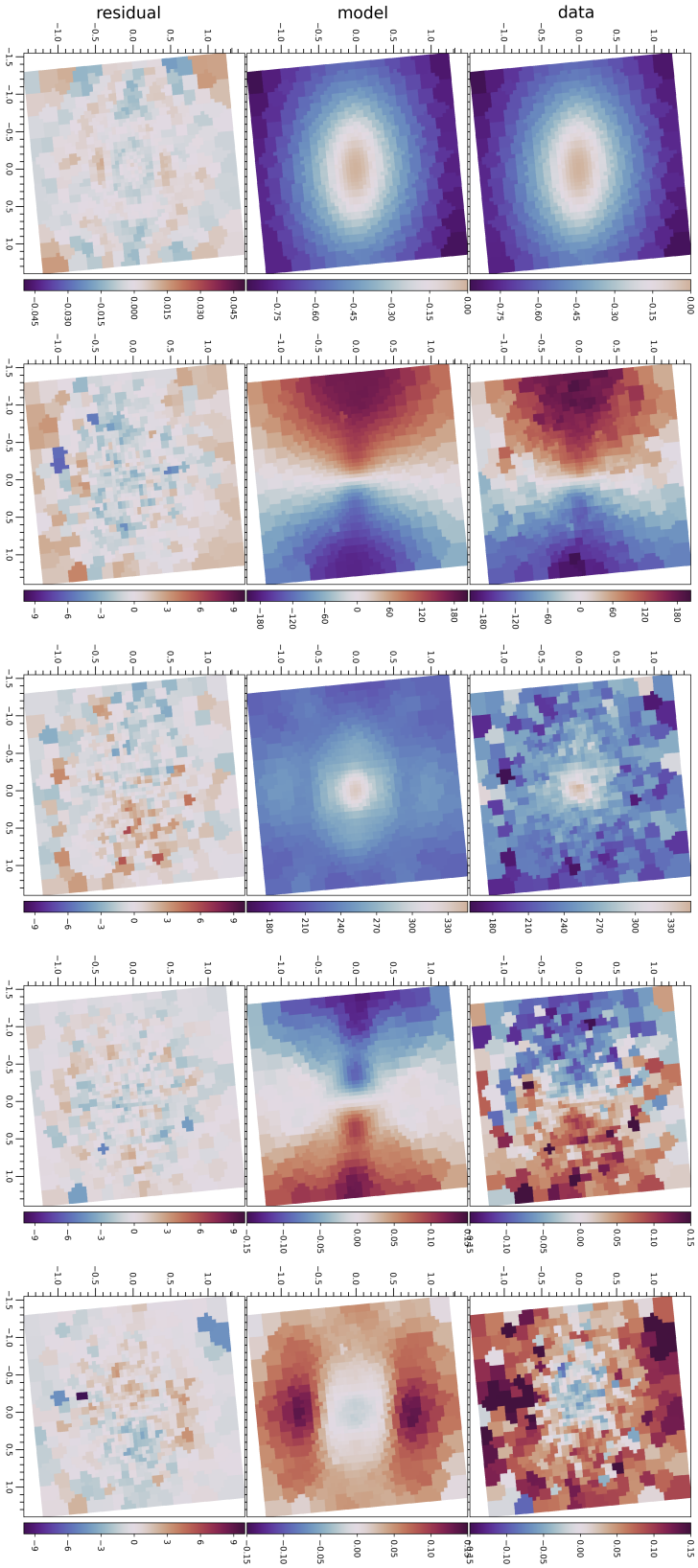

Figure A.4: This figure shows the kinematic maps for each kinematic moment for NGC 4281 from the high-resolution SINFONI data.

Bibliography

[1] Sabine Thater et al. “Six new supermassive black hole mass determinations from adaptive-optics assisted SINFONI observations”. In: *Astronomy & Astrophysics* 625 (May 2019), A62. DOI: 10.1051/0004-6361/201834808. URL: https://doi.org/10.1051%2F0004-6361%2F201834808.

[2] Edwin. Hubble. “No. 324. Extra-galactic nebulae.” In: *Contributions from the Mount Wilson Observatory / Carnegie Institution of Washington* 324 (Jan. 1926), pp. 1–49.

[3] Gerard de Vaucouleurs et al. *Third Reference Catalogue of Bright Galaxies*. 1991.

[4] C. Tohill et al. “A Robust Study of High-redshift Galaxies: Unsupervised Machine Learning for Characterizing Morphology with JWST up to z 8”. In: *The Astrophysical Journal* 962.2 (Feb. 2024), p. 164. ISSN: 1538-4357. DOI: 10.3847/1538-4357/ad17b8. URL: http://dx.doi.org/10.3847/1538-4357/ad17b8.

[5] Philipp Girichidis et al. “Physical Processes in Star Formation”. In: *Space Science Reviews* 216.4 (June 2020). ISSN: 1572-9672. DOI: 10.1007/s11214-020-00693-8. URL: http://dx.doi.org/10.1007/s11214-020-00693-8.

[6] Duncan Forbes. “Assembly Pathways and the Growth of Massive Early-Type Galaxies”. In: *Galaxies* 5.2 (2017). ISSN: 2075-4434. DOI: 10.3390/galaxies5020027. URL: https://www.mdpi.com/2075-4434/5/2/27.

[7] Gerard de Vaucouleurs. “Recherches sur les Nebuleuses Extragalactiques”. In: *Annales d’Astrophysique* 11 (Jan. 1948), p. 247.

[8] J. L. Sérsic. “Influence of the atmospheric and instrumental dispersion on the brightness distribution in a galaxy”. In: *Boletin de la Asociacion Argentina de Astronomia La Plata Argentina* 6 (Feb. 1963), pp. 41–43.

[9] R. C. E. van den Bosch et al. “Triaxial orbit based galaxy models with an application to the (apparent) decoupled core galaxy NGC 4365”. In: *Monthly Notices of the Royal Astronomical Society* 385.2 (Apr. 2008), pp. 647–666. DOI: 10.1111/j.1365-2966.2008.12874.x. arXiv: 0712.0113 [astro-ph].

[10] Yunpeng Jin et al. “Evaluating the ability of triaxial Schwarzschild modelling to estimate properties of galaxies from the Illustris simulation”. In: *Monthly Notices of the Royal Astronomical Society* 486.4 (July 2019), pp. 4753–4772. DOI: 10.1093/mnras/stz1170. arXiv: 1904.12942 [astro-ph.GA].

[11] Michele Cappellari. “Structure and Kinematics of Early-Type Galaxies from Integral Field Spectroscopy”. In: *Annual Review of Astronomy and Astrophysics* 54.1 (2016), pp. 597–665. DOI: 10.1146/annurev-astro-082214-122432. eprint: https://doi.org/10.1146/annurev-astro-082214-122432. URL: https://doi.org/10.1146/annurev-astro-082214-122432.

[12] Marta Reina-Campos et al. “Radial distributions of globular clusters trace their host dark matter halo: insights from the E-MOSAICS simulations”. In: *Monthly Notices of the Royal Astronomical Society* 513.3 (July 2022), pp. 3925–3945. DOI: 10.1093/mnras/stac1126. arXiv: 2106.07652 [astro-ph.GA].

[13] Meng Yang et al. “Dark matter measurements combining stellar and Hi kinematics: 30 percent 1 outliers with low dark matter content at 5Re”. In: *Monthly Notices of the Royal Astronomical Society* 528.3 (Feb. 2024), pp. 5295–5308. ISSN: 0035-8711. DOI: 10.1093/mnras/stae335. eprint: https://academic.oup.com/mnras/article-pdf/528/3/5295/56678745/stae335.pdf. URL: https://doi.org/10.1093/mnras/stae335.

[14] Tadeja Veršič et al. “Total mass slopes and enclosed mass constrained by globular cluster system dynamics”. In: *Astronomy amp; Astrophysics* 681 (Jan. 2024), A46. ISSN: 1432-0746. DOI: 10.1051/0004-6361/202347413. URL: http://dx.doi.org/10.1051/0004-6361/202347413.

[15] Event Horizon Telescope Collaboration et al. “First M87 Event Horizon Telescope Results. I. The Shadow of the Supermassive Black Hole”. In: 875.1, L1 (Apr. 2019), p. L1. DOI: 10.3847/2041-8213/ab0ec7. arXiv: 1906.11238 [astro-ph.GA].

[16] Event Horizon Telescope Collaboration et al. “First Sagittarius A* Event Horizon Telescope Results. III. Imaging of the Galactic Center Supermassive Black Hole”. In: *The Astrophysical Journal Letters* 930.2 (May 2022), p. L14. DOI: 10.3847/2041-8213/ac6429. URL: https://dx.doi.org/10.3847/2041-8213/ac6429.

[17] Aaron Smith, Volker Bromm, and Abraham Loeb. “The first supermassive black holes”. In: *Astronomy Geophysics* 58.3 (June 2017), pp. 3.22–3.26. ISSN: 1366-8781. DOI: 10.1093/astrogeo/atx099. eprint: https://academic.oup.com/astrogeo/article-pdf/58/3/3.22/17661140/atx099.pdf. URL: https://doi.org/10.1093/astrogeo/atx099.

[18] Michele Cappellari. “Measuring the inclination and mass-to-light ratio of axisymmetric galaxies via anisotropic Jeans models of stellar kinematics”. In: *Monthly Notices of the Royal Astronomical Society* 390.1 (Oct. 2008), pp. 71–86. DOI: 10.1111/j.1365-2966.2008.13754.x. arXiv: 0806.0042 [astro-ph].

[19] M. Schwarzschild. "A numerical model for a triaxial stellar system in dynamical equilibrium." In: *The Astrophysical Journal* 232 (Aug. 1979), pp. 236–247. DOI: 10.1086/157282.

[20] Edward M. Cackett, Misty C. Bentz, and Erin Kara. "Reverberation mapping of active galactic nuclei: From X-ray corona to dusty torus". In: *iScience* 24.6 (June 2021), p. 102557. ISSN: 2589-0042. DOI: 10.1016/j.isci.2021.102557. URL: http://dx.doi.org/10.1016/j.isci.2021.102557.

[21] Luka Č. Popović. In: *Open Astronomy* 29.1 (2020), pp. 1–14. DOI: doi:10.1515/astro-2020-0003. URL: https://doi.org/10.1515/astro-2020-0003.

[22] John Kormendy and Douglas Richstone. "Inward Bound—The Search For Supermassive Black Holes In Galactic Nuclei". In: *Annual Review of Astronomy and Astrophysics* 33 (Jan. 1995), p. 581. DOI: 10.1146/annurev.aa.33.090195.003053.

[23] Laura Ferrarese and David Merritt. "A Fundamental Relation between Supermassive Black Holes and Their Host Galaxies". In: *The Astrophysical Journal, Letters* 539.1 (Aug. 2000), pp. L9–L12. DOI: 10.1086/312838. arXiv: astro-ph/0006053 [astro-ph].

[24] Alister W. Graham et al. "A Correlation between Galaxy Light Concentration and Supermassive Black Hole Mass". In: *The Astrophysical Journal, Letters* 563.1 (Dec. 2001), pp. L11–L14. DOI: 10.1086/338500. arXiv: astro-ph/0111152 [astro-ph].

[25] John Kormendy and Luis C. Ho. "Coevolution (Or Not) of Supermassive Black Holes and Host Galaxies". In: *Anual Review of Astronomy and Astrophysics* 51.1 (Aug. 2013), pp. 511–653. DOI: 10.1146/annurev-astro-082708-101811. arXiv: 1304.7762 [astro-ph.CO].

[26] Alister W. Graham. "Galaxy Bulges and Their Massive Black Holes: A Review". In: *Galactic Bulges*. Ed. by Eija Laurikainen, Reynier Peletier, and Dimitri Gadotti. Vol. 418. Astrophysics and Space Science Library. Jan. 2016, p. 263. DOI: 10.1007/978-3-319-19378-6_11. arXiv: 1501.02937 [astro-ph.GA].

[27] Alister W. Graham and Nicholas Scott. "The M_{BH}-$L_{spheroid}$ Relation at High and Low Masses, the Quadratic Growth of Black Holes, and Intermediate-mass Black Hole Candidates". In: *The Astrophysical Journal* 764.2, 151 (Feb. 2013), p. 151. DOI: 10.1088/0004-637X/764/2/151. arXiv: 1211.3199 [astro-ph.CO].

[28] Remco C. E. van den Bosch. "Unification of the fundamental plane and Super Massive Black Hole Masses". In: *The Astrophysical Journal* 831.2, 134 (Nov. 2016), p. 134. DOI: 10.3847/0004-637X/831/2/134. arXiv: 1606.01246 [astro-ph.GA].

[29] Davor Krajnović, Michele Cappellari, and Richard M. McDermid. "Two channels of supermassive black hole growth as seen on the galaxies mass-size plane". In: *Monthly Notices of the Royal Astronomical Society* 473.4 (Feb. 2018), pp. 5237–5247. DOI: 10.1093/mnras/stx2704. arXiv: 1707.04274 [astro-ph.GA].

[30] James S. Bullock and Michael Boylan-Kolchin. "Small-Scale Challenges to the ΛCDM Paradigm". In: *Annual Review of Astronomy and Astrophysics* 55.1 (Aug. 2017), pp. 343–387. DOI: 10.1146/annurev-astro-091916-055313. arXiv: 1707.04256 [astro-ph.CO].

[31] L. Perivolaropoulos and F. Skara. "Challenges for ¡mml:math xmlns:mml="http://www.w3.org/1 altimg="si238.svg" display="inline" id="d1e11032"¿¡mml:mi mathvariant="normal"¿¡/mml:m An update". In: *New Astronomy Reviews* 95 (Dec. 2022), p. 101659. ISSN: 1387-6473. DOI: 10.1016/j.newar.2022.101659. URL: http://dx.doi.org/10.1016/j.newar.2022.101659.

[32] Prashin Jethwa et al. *DYNAMITE: DYnamics, Age and Metallicity Indicators Tracing Evolution*. Astrophysics Source Code Library, record ascl:2011.007. Nov. 2020. ascl: 2011.007.

[33] Sabine Thater et al. "Testing the robustness of DYNAMITE triaxial Schwarzschild modelling: The effects of correcting the orbit mirroring". In: *Astronomy and Astrophysics* 667, A51 (Nov. 2022), A51. DOI: 10.1051/0004-6361/202243926. arXiv: 2205.04165 [astro-ph.GA].

[34] Davor Krajnović et al. "A quartet of black holes and a missing duo: probing the low end of the M_{BH}-σ relation with the adaptive optics assisted integral-field spectroscopy". In: *Monthly Notices of the Royal Astronomical Society* 477.3 (July 2018), pp. 3030–3064. DOI: 10.1093/mnras/sty778. arXiv: 1803.08055 [astro-ph.GA].

[35] Sabine Thater et al. "Cross-checking SMBH mass estimates in NGC 6958 – I. Stellar dynamics from adaptive optics-assisted MUSE observations". In: *Monthly Notices of the Royal Astronomical Society* 509.4 (Nov. 2021), pp. 5416–5436. ISSN: 1365-2966. DOI: 10.1093/mnras/stab3210. URL: http://dx.doi.org/10.1093/mnras/stab3210.

[36] N. Nowak et al. "The supermassive black hole of FornaxA". In: *Monthly Notices of the Royal Astronomical Society* 391.4 (Dec. 2008), pp. 1629–1649. DOI: 10.1111/j.1365-2966.2008.13960.x. arXiv: 0809.0696 [astro-ph].

[37] Davor Krajnović et al. "Determination of masses of the central black holes in NGC 524 and 2549 using laser guide star adaptive optics". In: *Monthly Notices of the Royal Astronomical Society* 399.4 (Nov. 2009), pp. 1839–1857. DOI: 10.1111/j.1365-2966.2009.15415.x. arXiv: 0907.3748 [astro-ph.GA].

[38] Michele Cappellari et al. "The ATLAS^{3D} project - I. A volume-limited sample of 260 nearby early-type galaxies: science goals and selection criteria". In: *Monthly Notices of the Royal Astronomical Society* 413.2 (May 2011), pp. 813–836. DOI: 10.1111/j.1365-2966.2010.18174.x. arXiv: 1012.1551 [astro-ph.CO].

[39] Michele Cappellari and Yannick Copin. "Adaptive spatial binning of integral-field spectroscopic data using Voronoi tessellations". In: *Monthly Notices of the Royal Astronomical Society* 342.2 (June 2003), pp. 345–354. DOI: 10.1046/j.1365-8711.2003.06541.x. arXiv: astro-ph/0302262 [astro-ph].

[40] Michele Cappellari and Eric Emsellem. "Parametric Recovery of Line-of-Sight Velocity Distributions from Absorption-Line Spectra of Galaxies via Penalized Likelihood". In: *Publications of the Astronomical Society of the Pacific* 116.816 (Feb. 2004), pp. 138–147. DOI: 10.1086/381875. arXiv: astro-ph/0312201 [astro-ph].

[41] Michele Cappellari. "Improving the full spectrum fitting method: accurate convolution with Gauss-Hermite functions". In: *Monthly Notices of the Royal Astronomical Society* 466.1 (Apr. 2017), pp. 798–811. DOI: 10.1093/mnras/stw3020. arXiv: 1607.08538 [astro-ph.GA].

[42] A. Vazdekis et al. "Evolutionary stellar population synthesis with MILES - I. The base models and a new line index system". In: *Monthly Notices of the Royal Astronomical Society* 404.4 (June 2010), pp. 1639–1671. DOI: 10.1111/j.1365-2966.2010.16407.x. arXiv: 1004.4439 [astro-ph.CO].

[43] Cláudia Winge, Rogemar A. Riffel, and Thaisa Storchi-Bergmann. "The Gemini Spectral Library of Near-IR Late-Type Stellar Templates and Its Application for Velocity Dispersion Measurements". In: *The Astrophysical Journal-Supplement* 185.1 (Nov. 2009), pp. 186–197. DOI: 10.1088/0067-0049/185/1/186. arXiv: 0910.2619 [astro-ph.CO].

[44] Roeland P. van der Marel and Marijn Franx. "A New Method for the Identification of Non-Gaussian Line Profiles in Elliptical Galaxies". In: *The Astrophysical Journal* 407 (Apr. 1993), p. 525. DOI: 10.1086/172534.

[45] E. Emsellem, G. Monnet, and R. Bacon. "The multi-gaussian expansion method: a tool for building realistic photometric and kinematical models of stellar systems I. The formalism". In: *Astronomy and Astrophysics* 285 (May 1994), pp. 723–738.

[46] Douglas O. Richstone and Scott Tremaine. "Maximum-Entropy Models of Galaxies". In: *The Astrophysical Journal* 327 (Apr. 1988), p. 82. DOI: 10.1086/166171.

[47] Hans-Walter Rix et al. "Dynamical Modeling of Velocity Profiles: The Dark Halo around the Elliptical Galaxy NGC 2434". In: *The Astrophysical Journal* 488.2 (Oct. 1997), pp. 702–719. DOI: 10.1086/304733. arXiv: astro-ph/9702126 [astro-ph].

[48] Sabine Thater et al. "Effect of the initial mass function on the dynamical SMBH mass estimate in the nucleated early-type galaxy FCC 47". In: *Astronomy amp; Astrophysics* 675 (June 2023), A18. ISSN: 1432-0746. DOI: 10.1051/0004-6361/202245362. URL: http://dx.doi.org/10.1051/0004-6361/202245362.

[49] Aaron A. Dutton and Andrea V. Macciò. “Cold dark matter haloes in the Planck era: evolution of structural parameters for Einasto and NFW profiles”. In: *Monthly Notices of the Royal Astronomical Society* 441.4 (May 2014), pp. 3359–3374. ISSN: 0035-8711. DOI: 10.1093/mnras/stu742. URL: http://dx.doi.org/10.1093/mnras/stu742.

[50] Nicholas J. McConnell and Chung-Pei Ma. “Revisiting the Scaling Relations of Black Hole Masses and Host Galaxy Properties”. In: *The Astrophysical Journal* 764.2, 184 (Feb. 2013), p. 184. DOI: 10.1088/0004-637X/764/2/184. arXiv: 1211.2816 [astro-ph.CO].

[51] Alessandro Sonnenfeld et al. “Evidence for radial variations in the stellar mass-to-light ratio of massive galaxies from weak and strong lensing”. In: *Monthly Notices of the Royal Astronomical Society* 481.1 (Aug. 2018), pp. 164–184. ISSN: 1365-2966. DOI: 10.1093/mnras/sty2262. URL: http://dx.doi.org/10.1093/mnras/sty2262.